Abstracta

Ano XXVIII - N. 06

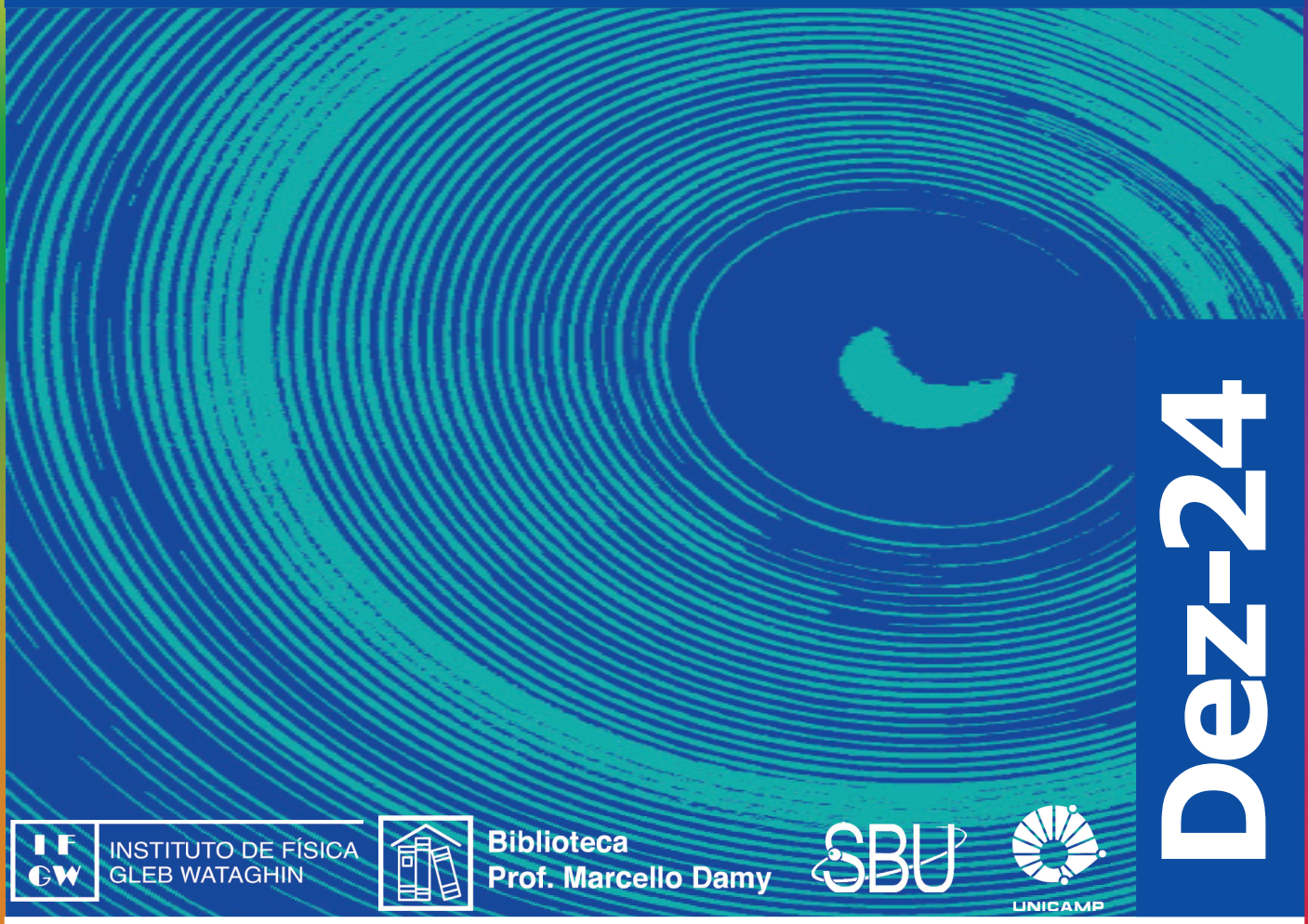

Artigos publicados

[P227-2024] "Acoustic Modulation of Excitonic Complexes in hBN/WSe2/hBN Heterostructures"

Gomes, M.L.F.*; Matrone, P. W.*; Cadore, A. R.; Santos, P. V.; **Couto, O. D. D. Jr*.**

The interaction of high-frequency surface acoustic waves (SAWs) and excitons in van der Waals heterostructures (vdWHs) offers challenging opportunities to explore novel quantum effects and functionalities. We probe the interaction of neutral excitons, trions, and biexcitons with SAWs in a hBN/WSe2/hBN vdWH. We show that neutral excitons respond weakly to the SAW stimulus at 5 K. The remaining excitonic complexes, because of their lower binding energy or charged character, interact much more efficiently with the SAW piezoelectric field, particularly intra- and intervalley trions. At room temperature, the SAW can play a dual role (sometimes dissociating excitons and sometimes increasing the vdWH local doping density) which depends of the laser-induced photodoping of the vdWH prior to the SAW generation and the role of metastable energy states in the SAW-induced carrier dynamics. Our results shed light in the unexplored biexciton modulation with SAWs, important for 2D materials-based optoelectronic and energy harvesting devices.

NANO LETTERS, 2024. DOI: 10.1021/acs.nanolett.4c03301. Early Access: NOV 2024

[P228-2024] "Agar-made biodegradable ball lens"

Rosa, L. O.; **Morais, E. F.*; Cordeiro, C. M. B.***; Fujiwara, E.

This work proposes the fabrication and characterization of ball lenses made of agar, a biodegradable and renewable material. Pouring a boiled solution of food-grade agar, glycerol, and water into cooled vegetable oil under agitation by a magnetic stirrer produces transparent and manipulable spheres. The glycerol concentration and rotation speed define the refractive index and size distribution, respectively, yielding lenses with diameters between 1 and 8 mm and indices ranging from 1.33 to 1.46. Experiments also characterized the output beam profile with 632 nm laser illumination. The results corroborate with the focal length simulated for a Gaussian beam model, suggesting controllable optical properties and anticipating potential applications of the agar ball lens as a biodegradable optical device for biomedical imaging, illumination, and sensing.

APPLIED OPTICS 63[30], 8028-8033, 2024. DOI: 10.1364/AO.534801

[P229-2024] "ALICE upgrades during the LHC Long Shutdown 2"

Acharya, S.; Hernandez, R. A.; Adamová, D.; **Chinellato, D. D.*; Guardiano, G. G.*; Jahnke, C.*; Takahashi, J.***; et al. ALICE Collaboration

A Large Ion Collider Experiment (ALICE) has been conceived and constructed as a heavy-ion experiment at the LHC. During LHC Runs 1 and 2, it has produced a wide range of physics results using all collision systems available at the LHC. In order to best exploit new physics opportunities opening up with the upgraded LHC and new detector technologies, the experiment has undergone a major upgrade during the LHC Long Shutdown 2 (2019-2022). This comprises the move to continuous readout, the complete overhaul of core detectors, as well as a new online event processing farm with a redesigned online-offline software framework. These improvements will allow to record Pb-Pb collisions at rates up to 50 kHz, while ensuring sensitivity for signals without a triggerable signature.

JOURNAL OF INSTRUMENTATION 19[5], P05062, 2024. DOI: 10.1088/1748-0221/19/05/P05062

[P230-2024] "An Impedance Humidity Sensor Based on CVD Grown WSe2 2D Films"

Bhadra, J.; Sassi, L. M.; **Oliveira, E. F.***; Hachtel, J. A.; Parangusan, H.; Mallick, S. A.; Ahmad, Z.; **Galvao, D. S.***; Puthirath, A. B.; Vajtai, R.; Ajayan, P. M.; Al-Thani, N.

2D materials-based planar devices have been sought after for gas and humidity sensor applications owing to their high sensitivity due to their ultrathin nature and increased surface area. Herein, 2D WSe2 films-based planner devices were fabricated to evaluate their performance for potential application in humidity sensors. The structure and morphology of the WSe2 sensing films were studied by Raman spectroscopy, photoluminescence, optical microscopy, and scanning electron microscopy (SEM) techniques. The relative humidity-dependent sensing performances of the 2D WSe2 films were evaluated using current-voltage (I-V), relative impedance, and complex total impedance (electrochemical impedance spectroscopy, EIS) techniques. This sensor showed a very stable and repeatable performance investigated over the period of 18 months. The response and recovery times of the WSe2-based impedance sensors were found to be 40 and 30 s, respectively. The WSe2 sensor exhibits a 2 +/- 1% minimum hysteresis at a lower humidity level (50% RH) and around 8 +/- 2% maximum hysteresis at relative humidity level (70% RH). This value of hysteresis is in the acceptable range during the initial investigation of any material to explore its potential for application in humidity sensors. The density functional theory (DFT) analysis was performed with the interaction from water molecules of the WSe2 sample for a better understanding of the sensing mechanism of devices.

ACS APPLIED ELECTRONIC MATERIALS 6[11], 7734-7743, 2024. DOI: 10.1021/acsaelm.4c00863

[P231-2024] "Assessing biological self-organization patterns using statistical complexity characteristics: a tool for diffusion tensor imaging analysis"

Senra Filho, A. C. da S.*; Murta Junior, L. O.; **Paschoal, A. M.***

ObjectDiffusion-weighted imaging (DWI) and diffusion tensor imaging (DTI) are well-known and powerful imaging techniques for MRI. Although DTI evaluation has evolved continually in recent years, there are still struggles regarding quantitative measurements that can benefit brain areas that are consistently difficult to measure via diffusion-based methods, e.g., gray matter (GM). The present study proposes a new image processing technique based on diffusion distribution evaluation of L & oacute;pez-Ruiz, Mancini and Calbet (LMC) complexity called diffusion complexity (DC).Materials and MethodsThe OASIS-3 and TractoInferno open-science databases for healthy individuals were used, and all the codes are provided as open--source materials.ResultsThe DC map showed relevant signal characterization in brain tissues and structures, achieving contrast-to-noise ratio (CNR) gains of approximately 39% and 93%, respectively, compared to those of the FA and ADC maps. DiscussionIn the special case of GM tissue, the DC map obtains its maximum signal level, showing the possibility of studying cortical and subcortical structures challenging for classical DTI quantitative formalism. The ability to apply the DC technique, which requires the same imaging acquisition for DTI and its potential to provide complementary information to study the brain's GM structures, can be a rich source of information for further neuroscience research and clinical practice.

MAGNETIC RESONANCE MATERIALS IN PHYSICS BIOLOGY AND MEDICINE, 2024. DOI: 10.1007/s10334-024-01185-4. Early Access Date: JUL 2024

[P232-2024] "Charge Trapping and Detrapping in CsPbBr3 Perovskite Nanocrystals: Implications for Photovoltaic and Photocatalysis Applications"

Vale, B. R. C.*; Scolfaro, D.*; Sousa, C. A.*; Fonseca, A. F. V. **Bonato, L. G.*;** Nogueira, A. F.; Bettini, J .; **Padilha, L. A*.**

Perovskite nanocrystals (PNCs) have emerged as a promising platform for the development of highly efficient nanomaterial-based lighting devices. Although experiments and calculations have shown that defect densities are on the order of 1011-1016 cm-3 in bulk perovskites, this is not true for nanomaterials because they present higher defect densities. To understand the origin and relative contribution of those defects, we employed transient absorption spectroscopy and time-resolved photoluminescence. We scrutinize the exciton dynamics in PNCs for over 7 orders of magnitude in time, and we conclude that, in the ensemble of CsPbBr3 PNCs, excited carriers can take different paths to return to the fundamental level: electron traps (hundreds of picoseconds), surface traps (2-5 ns), direct radiative recombination (similar to 10 ns), and delayed emission. Our measurements revealed that the excitonic component of PNCs tends to decrease with increasing nanocrystal (NC) size. On the other hand, we observed that the electron trap decay amplitude correlates with the relative delayed emission contribution, suggesting that the recombination of detrapped species comes from electron-trapping sites. Besides, the relative contribution of delayed emission is size-dependent and increases with the NC size, achieving about 80% of reversibility. Although the excitonic contribution of larger NCs is lower compared to the smaller ones, the results suggest that electron traps are reversible and do not decrease the photoluminescence quantum yield of the NCs. These results can be useful for applications that involve charge-carrier extraction, such as photovoltaics and photocatalysis.

ACS APPLIED NANO MATERIALS, 2024. DOI: 10.1021/acsanm.4c04839. Early Access NOV 2024

[P233-2024] "Combination of Measurements of the Top Quark Mass from Data Collected by the ATLAS and CMS Experiments at √s=7 and 8 TeV"

Hayrapetyan, A.; Tumasyan, A.; Adam, W.; **Chinellato, J. A.***; et al.
CMS Collaboration; ATLAS Collaboration

A combination of fifteen top quark mass measurements performed by the ATLAS and CMS experiments at the LHC is presented. The datasets used correspond to an integrated luminosity of up to 5 and 20 fb(-1) of proton-proton collisions at center-of-mass energies of 7 and 8 TeV, respectively. The combination includes measurements in top quark pair events that exploit both the semileptonic and hadronic decays of the top quark, and a measurement using events enriched in single top quark production via the electroweak t channel. The combination accounts for the correlations between measurements and achieves an improvement in the total uncertainty of 31% relative to the most precise input measurement. The result is m(t) = 172.52 +/- 0.14(stat) +/- 0.30(stat) GeV, with a total uncertainty of 0.33 GeV.

PHYSICAL REVIEW LETTERS 132[26] 261902, 2024. DOI: 10.1103/PhysRevLett.132.261902

[P234-2024] "Combined search for electroweak production of winos, binos, higgsinos, and sleptons in proton-proton collisions at √s=13 TeV"

Hayrapetyan, A.; Tumasyan, A.; Adam, W.; **Chinellato, J. A.***; et al.
CMS Collaboration

A combination of the results of several searches for the electroweak production of the supersymmetric partners of standard model bosons, and of charged leptons, is presented. All searches use proton-proton collision data at root s = 13 TeV recorded with the CMS detector at the LHC in 2016-2018. The analyzed data correspond to an integrated luminosity of up to 137 fb(-1). The results are interpreted in terms of simplified models of supersymmetry. Two new interpretations are added with this combination: a model spectrum with the bino as the lightest supersymmetric particle together with mass-degenerate Higgsinos decaying to the bino and a standard model boson, and the compressed-spectrum region of a previously studied model of slepton pair production. Improved analysis techniques are employed to optimize sensitivity for the compressed spectra in the wino and slepton pair production models. The results are consistent with expectations from the standard model. The combination provides a more comprehensive coverage of the model parameter space than the individual searches, extending the exclusion by up to 125 GeV, and also targets some of the intermediate gaps in the mass coverage.

PHYSICAL REVIEW D 109[11], 112001, 2024. DOI: 10.1103/PhysRevD.109.112001

[P235-2024] "Comparison of Blue and Infrared Light Transmission Through Dental Tissues and Restorative Materials"

Pacheco, R. R.; **Garcia-Flores, A. F.*; Lesseux, G. G.*; Lancelotti, A.*; Rettori, C.*; Urbano, R. R. *; Giannini, M.*;** Rueggeberg, F. A.;

Objectives: The depth of cure using blue -light photocuring units (BL) is limited by tooth structure and qualities of the restorative material through which the activating wavelength must pass. Recent developments incorporate an infrared (IR) activated upconversion (UC) fluorescence of a lining agent filled with nanocrystals of NaYF 4 and doped with YB +3 and Tm +3 that emit both blue and violet light locally at the interface of the liner and restorative resin. The purpose of this study was to evaluate the BL and 975 nm infrared (IR) light power transmission through dental tissues and restorative materials. Methods and Materials: Power transmissions of the IR laser (975 nm) and a monowave blue -only lightcuring unit (Bluephase 16i) through dental tissues (enamel, dentin, and enamel/dentin junction, or DEJ), eight (8) various dental resin composites, and eight (8) dental ceramics, each at four thicknesses (1, 2, 3 and 4 mm) were evaluated (n=5) using a thermopile sensor (PM10, Coherent Inc) connected to a laser power meter (Fieldmate, Coherent Inc). Power transmission values of each light source and restorative material were subjected to analysis of variance and Tukey test at a pre-set alpha of 0.05.Results: A linear correlation (r=0.9884) between the supplied current and emitted IR power of the laser diode was found, showing no statistical power reduction with increased distances (collimated beam). For tooth tissues, the highest power transmissions for both light sources were observed using 1.0 mm enamel while the lowest values were found for 2.0 mm dentin and an association of 2.0 mm DEJ and 1.0 mm dentin. The only group where IR demonstrated significantly higher transmission when compared to BL was 1.0 mm enamel. For all resin composites and dental ceramics, increased thickness resulted in a reduction of IR power transmission (except for EverX Posterior fiberreinforced composite and e.max HT ceramic).IR resulted in higher transmission through all resin composites, except for Tetric EvoCeram White. The highest BL transmission was observed for SDR Flow, at all thicknesses. Higher IR/BL ratios were observed for EverX Posterior, Herculite Ultra, and Lava Ultimate, while the lowest ratio was observed for Tetric EvoCeram White. Reduced translucency shades within the same material resulted in lower power ratio values, especially for BL transmission. Higher IR/BL ratios were observed for e.Max LT, VitaVM7 Base Dentin, and e.max CAD HT, while the lowest values were found for VitaVM7 Enamel and Paradigm C.

Conclusion: IR power transmission through enamel was higher when compared to blue light, while no difference was observed for dentin. The power transmission of IR was higher than BL for resin composites, except for a high value and low chroma shade. Fiber -reinforced resin composite demonstrated the highest IR/BL power transmission ratio. A greater IR/BL ratio was observed for lower translucency ceramics when compared to high translucency.

OPERATIVE DENTISTRY 49[3], 300-310, 2024. DOI: 10.2341/23-056-LN

[P236-2024] "Corrosion behaviour of the Ti-6Al-4V alloy after functionalization by polyacrylic acid using plasma--enhanced chemical vapor deposition"

Teixeira, G. T. L.; Ferreira, M. O. A.; Gelamo, R. V.; Obata, M. M. S.; Perini, H. F.; Silva, M. V. da; **Siervo, A. de*;** Slade, G. G.; Moreto, J. A.; Slade, N. B. L.

The plasma-enhanced chemical vapor deposition (PECVD) technique emerges as a versatile approach for the functionalization of metallic materials, offering the capability to produce coatings endowed with antimicrobial properties, good biocompatibility, and enhanced resistance to corrosion processes. In this study, we investigated the efficacy of a thin plasma polymer based on polyacrylic acid (PAA) film coated onto Ti-6Al-4V alloy via the PECVD technique in inhibiting uniform corrosion processes and exerting antibacterial activity. The electrochemical behaviour was accessed by using open circuit potential (OCP), potentiodynamic polarization (PP) and electrochemical impedance spectroscopy (EIS) in 0.6 mol L-1 NaCl solution. X--ray photoelectron spectroscopy (XPS) technique was used to characterize the thin film produced in the metallic surfaces. It also confirmed that PECVD was advantageous for producing the PAA coating onto Ti-6Al-4V surface by presenting a thickness of about 180 nm, determined through AFM technique. The electrochemical results demonstrated that the PAA coatings act as protective barrier, improving the corrosion resistance of the Ti-6Al-4V alloy. Contact angle measurements and surface free energy analysis revealed a decrease in surface wettability induced by the PAA deposition process. Biological tests evaluating antibiofilm activity demonstrated a reduction of 70% and 60% in the adhesion of Escherichia coli (E. coli) and Staphylococcus aureus (S. aureus) bacteria, respectively, compared to the bare material, while preserving cell viability. These findings highlight the inhibitory properties of the developed material, providing a proof of concept for an innovative, practical material with a wide range of potential applications. The functionalization process shows potential for enabling a more aseptic and safer implantation procedure, leading to an extended lifespan compared to the bare material. This broadens the scope of applications for the Ti-6Al-4V alloy in the biomedical field.

EMERGENT MATERIALS 7[5], 2143-2161, 2024. DOI: 10.1007/s42247-024-00739-5

[P237-2024] "Cosmological shocks around galaxy clusters: a coherent investigation with DES, SPT, and ACT"

Anbajagane, D.; Chang, C.; Baxter, E. J.; **Navarro-Alsina, A.***; et al.

We search for signatures of cosmological shocks in gas pressure profiles of galaxy clusters using the cluster catalogues from three surveys: the Dark Energy Survey (DES) Year 3, the South Pole Telescope (SPT) SZ survey, and the Atacama Cosmology Telescope (ACT) data releases 4, 5, and 6, and using thermal Sunyaev-Zeldovich (SZ) maps from SPT and ACT. The combined cluster sample contains around 10(5) clusters with mass and redshift ranges 10(13.7) < M--200m/ M-circle dot < 10(15.5) and 0.1 < z < 2, and the total sky coverage of the maps is approximate to 15 000 deg(2). We find a clear pressure deficit at R/R-200m approximate to 1.1 in SZ profiles around both ACT and SPT clusters, estimated at 6 sigma significance, which is qualitatively consistent with a shock-induced thermal non-equilibrium between electrons and ions. The feature is not as clearly determined in profiles around DES clusters. We verify that measurements using SPT or ACT maps are consistent across all scales, including in the deficit feature. The SZ profiles of optically selected and SZ-selected clusters are also consistent for higher mass clusters. Those of less massive, optically selected clusters are suppressed on small scales by factors of 2-5 compared to predictions, and we discuss possible interpretations of this behaviour. An oriented stacking of clusters - where the orientation is inferred from the SZ image, the brightest cluster galaxy, or the surrounding large-scale structure measured using galaxy catalogues - shows the normalization of the one-halo and two-halo terms vary with orientation. Finally, the location of the pressure deficit feature is statistically consistent with existing estimates of the splashback radius.

MONTHLY NOTICES OF THE ROYAL ASTRONOMICAL SOCIETY 527[3], 9378-9404, 2024. DOI: 10.1093/mnras/stad3726

[P238-2024] "Crystal structure and cryomagnetic study of a mononuclear erbium(III) oxamate inclusion complex"

Araujo Junior, C. R.; Oliveira, W. X. C.; Pinheiro, C. B.; Pedroso, E. F.; Nunes, W. C.; **Almeida, A. A. de*; Knobel, M.***; Julve, M.; Pereira, C. L. M.

The synthesis, crystal structure and magnetic properties of an oxamate-containing erbium(III) complex, namely, tetrabutylammonium aqua[N-(2,4,6-trimethylphenyl)oxamato] erbium(III)-dimethyl sulfoxide-water (1/3/1.5), (C16H36N)--[Er(C11H12NO3)(4)(H2O)]center dot 3C(2)H(6)OS center dot 1.5H(2)O or n-Bu4N-[Er(Htmpa)(4)(H2O)]center dot-3DMSO center dot 1.5H(2)O (1), are reported. The crystal structure of 1 reveals the occurrence of an erbium(III) ion, which is surrounded by four N-phenyl-substituted oxamate ligands and one water molecule in a nine-coordinated environment, together with one tetrabutylammonium cation acting as a counterion, and one water and three dimethyl sulfoxide (DMSO) molecules of crystallization. Variable-temperature static (dc) and dynamic (ac) magnetic measurements were carried out for this mononuclear complex, revealing that it behaves as a field-induced single-ion magnet (SIM) below 5.0 K.

ACTA CRYSTALLOGRAPHICA SECTION C-STRUCTURAL CHEMISTRY 80, 349-+, 2024. DOI: 10.1107/S2053229624005977

[P239-2024] "Development of the CMS detector for the CERN LHC Run 3"

Hayrapetyan, A.; Tumasyan, A.; Adam, W.; **Chinellato, J. A.*** et al.
CMS Collaboration

Since the initial data taking of the CERN LHC, the CMS experiment has undergone substantial upgrades and improvements. This paper discusses the CMS detector as it is configured for the third data-taking period of the CERN LHC, Run 3, which started in 2022. The entire silicon pixel tracking detector was replaced. A new powering system for the superconducting solenoid was installed. The electronics of the hadron calorimeter was upgraded. All the muon electronic systems were upgraded, and new muon detector stations were added, including a gas electron multiplier detector. The precision proton spectrometer was upgraded. The dedicated luminosity detectors and the beam loss monitor were refurbished. Substantial improvements to the trigger, data acquisition, software, and computing systems were also implemented, including a new hybrid CPU/GPU farm for the high-level trigger.

JOURNAL OF INSTRUMENTATION 19[5], P05064, 2024. DOI: 10.1088/1748-0221/19/05/P05064

[P240-2024] "Enhanced performance of impedimetric immunosensors to detect SARS-CoV-2 with bare gold nanoparticles and graphene acetic acid"

Hensel, R. C.; Di Vizio, B.; Materòn, E. M.; **Shimizu, F. M.***; Angelim, M. K. S. C.; Souza, G. F. de; Módena, J. L. P.; Moraes-Vieira, P. M. M.; Azevedo, R. B. de; Litti, L.; Agnoli, S.; Casalini, S.; Oliveira Jr., O. N.

Immunosensors based on electrical impedance spectroscopy allow for label-free, real-time detection of biologically relevant molecules and pathogens, without requiring electro-active materials. Here, we investigate the influence of bare gold nanoparticles (AuNPs), synthesized via laser ablation in solution, on the performance of an impedimetric immunosensor for detecting severe acute respiratory syndrome coronavirus (SARS-CoV-2). Graphene acetic acid (GAA) was used in the active layer for immobilizing anti-SARS-CoV-2 antibodies, owing to its high density of carboxylic groups. Immunosensors incorporating AuNPs exhibited superior performance compared to those relying solely on GAA, achieving a limit of detection (LoD) of 3 x 10-20 g/mL to detect the Spike Receptor Binding Domain (RBD) protein of SARS-CoV-2 and of 2 PFU/mL for inactivated virus. Moreover, these immunosensors presented high selectivity against the H1N1 influenza virus. We anticipate that this platform will be versatile and applicable in the early diagnosis of various diseases and viral infections, thereby facilitating Point-of-Care testing.

TALANTA 281, 126903, 2024. DOI: 10.1016/j.talanta.2024.126903

[P241-2024] "Enhancing the light yield of He:CF4 based gaseous detector"

Amaro, F. D.; Antonietti, R.; Baracchini, E.; **Kemp, E.***; et al.

The CYGNO experiment aims to build a large (O(10)m(3)) directional detector for rare event searches, such as nuclear recoils (NRs) induced by dark matter (DM), such as weakly interactive massive particles (WIMPs). The detector concept comprises a time projection chamber (TPC), filled with a He:CF4 60/40 scintillating gas mixture at room temperature and atmospheric pressure, equipped with an amplification stage made of a stack of three gas electron multipliers (GEMs) which are coupled to an optical readout. The latter consists in scientific CMOS (sCMOS) cameras and photomultipliers tubes (PMTs). The maximisation of the light yield of the amplification stage plays a major role in the determination of the energy threshold of the experiment. In this paper, we simulate the effect of the addition of a strong electric field below the last GEM plane on the GEM field structure and we experimentally test it by means of a 10 cm(2) readout area prototype. The experimental measurements analyse stacks of different GEMs and helium concentrations in the gas mixture combined with this extra electric field, studying their performances in terms of light yield, energy resolution and intrinsic diffusion. It is found that the use of this additional electric field permits large light yield increases without degrading intrinsic characteristics of the amplification stage with respect to the regular use of GEMs.

EUROPEAN PHYSICAL JOURNAL C 84[10], 1122, 2024. DOI: 10.1140/epjc/s10052-024-13471-5

[P242-2024] "Evaluation and synthesis of perovskite crystals as high-Z sensors for hybrid pixel detectors"

Campanelli, R. B.*; Gomes, G. S.; Donatti, M. M.; Perissinotto, L. S.; Pereira, A. D.; Antonio, E. B.; Vincoletto, P. L.; Fernandes, M. G.; Araujo, L. S.; Polli, J. M.; **Marques, F. C.***

High-energy photon imaging experiments are crucial techniques in synchrotron facilities, often employing hybrid pixel detectors for these operations. These detectors combine a photo-sensitive semiconductor component with a pixelated microelectronic Application Specific Integrated Circuit (ASIC) for signal processing and image formation. However, detecting photons above 90 keV poses significant challenges, even for heavy semiconductors, due to lower photoelectric absorption crosssection at this energy range. Nevertheless, lead-based perovskites, such as CsPbBr3, are remarkable alternatives as they present excellent cross-section values and noteworthy transport properties, contributing to increased high-energy detection efficiencies. Here, we employ a chemical synthesis route for CsPbBr3 single-crystals, enabling experimental measurements of carrier mobility of 100.7 cm2 /Vs. We also developed a simulation algorithm to calculate the current pulses generated on pixelated electrodes. Our simulations evaluate CsPbBr3's performance coupled with the latest photon-counter ASIC developed by CERN, the Timepix4. Our findings indicate that CsPbBr3 crystals require intense applied electric fields, around 1 kV/mm, for accurate signal integration. Furthermore, we observed no correlation between incident energy and induced pulse width. Through microelectronics simulations, we demonstrate that the signal formation behavior of CsPbBr3 is compatible with Timepix4 ASICs, consequently establishing operational guidelines for employing this promising material as sensors in hybrid pixel detectors.

SCIENTIFIC REPORTS 14[1], 27430, 2024. DOI: 10.1038/s41598-024-74384-7

[P243-2024] "Evaluation of Antibacterial Activity of Bismuth Ferrites Nanoparticles in the Inhibition of E. Coli and S. Aureus Bacteria"

Pancotti, A.; Souza, M. V. de B.; Abreu, A. S.; Rezende, S. R.; Moreli, M. L.; Otero, E. U.; **Landers, R.***; Soares, R.; Wang, J. L.

In this work, bismuth ferrites (BFO) nanoparticles were produced in the form of using sol-gel technique, followed by annealing in a tube furnace in temperatures from 400 degrees C to 650 degrees C. X-ray diffraction (XRD) results showed the formation of small sizes nanoparticles (NPs) with high purity. Structural analysis displayed that annealing at 600 degrees C could make BFO NPs be fitted to rhombohedral space group (R3c), with small quantity of spurious phases. The sizes of the BFO nanoparticles determined by transmission electron microscopy (HRTEM) are between 50 to 100 nm. To evaluate the efficiency of BFO in antimicrobial susceptibility tests, the nanoparticles were dispersed through cand tested agar diffusion method and dilution in a 96 well plate using a Gram-positive strains (Staphylococcus aureus) and Gram negative strain (Escherichia coli). The antibacterial activity of the BFO NPs was tested at concentrations of 2 mg/mL with MIC greater than 60 mu g/mL for both bacteria.

CHEMISTRY & BIODIVERSITY, 2024. DOI: 10.1002/cbdv.202402048 Early Access Date: NOV 2024

[P244-2024] "Extracting the speed of sound in quark-gluon plasma with ultrarelativistic lead-lead collisions at the LHC"

Hayrapetyan, A.; Tumasyan, A.; Adam, W.; **Chinellato, J. A.***; et al.
CMS Collaboration

Ultrarelativistic nuclear collisions create a strongly interacting state of hot and dense quark-gluon matter that exhibits a remarkable collective flow behavior with minimal viscous dissipation. To gain deeper insights into its intrinsic nature and fundamental degrees of freedom, we determine the speed of sound in an extended volume of quark-gluon plasma using lead-lead (PbPb) collisions at a center-of-mass energy per nucleon pair of 5.02 TeV. The data were recorded by the CMS experiment at the CERN LHC and correspond to an integrated luminosity of 0.607 nb(-1). The measurement is performed by studying the multiplicity dependence of the average transverse momentum of charged particles emitted in head-on PbPb collisions. Our findings reveal that the speed of sound in this matter is nearly half the speed of light, with a squared value of 0.241 +/- 0.002 (stat) +/- 0.016 9(syst) in natural units. The effective medium temperature, estimated using the mean transverse momentum, is 219 +/- 8 The measured squared speed of sound at this temperature aligns precisely with predictions from lattice quantum chromodynamic (QCD) calculations. This result provides a stringent constraint on the equation of state of the created medium and direct evidence for a deconfined QCD phase being attained in relativistic nuclear collisions.

REPORTS ON PROGRESS IN PHYSICS 87[7], 077801, 2024. DOI: 10.1088/1361-6633/ad4b9b

[P245-2024] "Functional near- infrared spectroscopy: A novel tool for detecting consciousness after acute severe brain injury"

Kazazian, K.; Abdalmalak, A.; Novi, S. L.; Norton, L.; Ardakani, R. M.; Kolisnyk, M.; Gofton, T. E.; **Mesquita, R. C.***; Owen, A. M.; Debicki, D. B.

Recent advancements in functional neuroimaging have demonstrated that some unresponsive patients in the intensive care unit retain a level of consciousness that is inconsistent with their behavioral diagnosis of awareness. Functional near-infrared spectroscopy (fNIRS) is a portable optical neuroimaging method that can be used to measure neural activity with good temporal and spatial resolution. However, the reliability of fNIRS for detecting the neural correlates of consciousness remains to be established. In a series of studies, we evaluated whether fNIRS can record sensory, perceptual, and command- driven neural processing in healthy participants and in behaviorally nonresponsive patients. At the individual healthy subject level, we demonstrate that fNIRS can detect commonly studied resting state networks, sensorimotor processing, speech- specific auditory processing, and volitional command- driven brain activity to a motor imagery task. We then tested fNIRS with three acutely brain injured patients and found that one could willfully modulate their brain activity when instructed to imagine playing a game of tennis-providing evidence of preserved consciousness despite no observable behavioral signs of awareness. The successful application of fNIRS for detecting preserved awareness among behaviorally nonresponsive patients highlights its potential as a valuable tool for uncovering hidden cognitive states in critical care settings.

PROCEEDINGS OF THE NATIONAL ACADEMY OF SCIENCES OF THE UNITED STATES OF AMERICA 121[36], e2402723121, 2024. DOI: 10.1073/pnas.2402723121

[P246-2024] "Hanbury-Brown and Twiss effect in inflationary cosmological perturbations"

Gauy, G. M.*; Sobreira, F.*; Torrieri, G.*

The simplest model of inflation is based around an inflaton field that starts in a coherent false vacuum state with a positive cosmological constant, rolls slowly to the true vacuum and relaxes to it via reheating. We examine whether the scale of the transition from coherence to chaoticity can be examined via the Hanbury-Brown and Twiss (HBT) effect, in parallel with analogous problems of heavy ion physics (the "pion laser" and the thermalizing glasma). We develop an ansatz which contains a definition of "chaoticity" which parallels that of the usual setups where HBT is used. However, we also discuss the differences between the inflationary setup and more mainstream uses of HBT and conclude that these are more significant than the similarities, making the use of the developed methodology uncertain.

PHYSICAL REVIEW D 110[8], 083521, 2024. DOI: 10.1103/PhysRevD.110.083521

[P247-2024] "High-Temperature Sensing Using a Hollow--Core Fiber With Thick Cladding Tubes"

Rodrigues, G. L.*; Cordeiro, C. M. B.*; Amrani, F.; Gérôme, F.; Benabid, F.; **Osório, J. H.***

We report on high-temperature sensing measurements using a tubular-lattice hollow-core photonic crystal fiber (HCPCF) displaying a microstructure formed of eight 2.4-mu m-thick cladding tubes. The larger thickness of our fiber's cladding tubes compared to other hollow fibers operating in the visible and infrared ranges entails multiple narrow transmission bands in its transmission spectrum (six bands in the spectral range between 400 and 950 nm) and benefits the realization of the temperature sensing measurements. The principle of operation of our device is based on the thermo-optic effect and thermal expansion-induced spectral shifts of the fiber transmission bands due to temperature variations. To study the sensor operation, we monitored the fiber transmission bands' spectral positions from room temperature to 1085 degree celsius in both ramp-up and ramp-down scenarios. Additionally, we investigated the optimization opportunities by assessing an analytical model describing the fiber transmission characteristics and discussed the alternatives for enhancing the sensor performance. Moreover, our fiber characterization experiments revealed a consistent confinement loss (CL) trend aligned with the scaling laws in tubular-lattice hollow-core fibers. We thus understand that the results presented in this article highlight a relevant path for the development of temperature sensors based on microstructured hollow-core optical fibers endowed with thick cladding tubes.

IEEE SENSORS JOURNAL 24[16], 25769-25776, 2024. DOI: 10.1109/JSEN.2024.3421896

[P248-2024] "Highly Amplified Broadband Ultrasound in Antiresonant Hollow Core Fibers"

Silva, R. E. da; Webb, D. J.; **Cordeiro, C. M. de B.*;** Franco, M. A. R.

High-frequency broadband ultrasound in nested antiresonant hollow core fibers (NANFs) is investigated for the first time. NANFs have remarkable features enabling high-resolution microscale optoacoustic imaging sensors and neurostimulators. Solid optical fibers have been successfully employed to measure and generate ultrasonic signals, however, they face issues concerning attenuation, limited frequency range, bandwidth, and spatial resolution. Herein, highly efficient ultrasonic propagation in NANFs from 10 to 100 MHz is numerically demonstrated. The induced pressures and sensing responsivity are evaluated in detail, and important parameters for the development of ultrasonic devices are reviewed. High pressures (up to 234 MPa) and sensing responsivities (up to -207 dB) are tuned over 90 MHz range by changing the diameters of two distinct NANF geometries. To the best of knowledge, this is the widest bandwidth reported using similar diameter fibers. The results are a significant advance for fiber-based ultrasonic sensors and transmitters,

contributing to improve their efficiency and microscale spatial resolution for the detection, diagnosis, and treatment of diseases in biomedical applications. Highly efficient ultrasound propagation in antiresonant hollow core fibers is demonstrated from 10 to 100 MHz. Significant pressures (up to 234 MPa) and sensing responsivities (up to -207 dB) are tuned over a 90 MHz broadband range by adjusting the fiber geometry. These achievements are promising for optoacoustic sensors and neurostimulators, improving spatial resolution to treat diseases in biomedical applications.

ADVANCED PHOTONICS RESEARCH, 2024. DOI: 10.1002/adpr.202400086. Early Access Date: OCT 2024

[P249-2024] "Highly anisotropic superconducting gap near the nematic quantum critical point of FeSe1-xSx"

Nag, P. K.; Scott, K.; Carvalho, V. S. de; Byland, J. K.; Yang, X. Z.; Walker, M.; Greenberg, A. G.; Klavins, P.; **Miranda, E.***; Gozar, A.; Taufour, V.; Fernandes, R. M.; Neto, E. H. da S.

Nematic phases, in which electrons in a solid spontaneously break rotational symmetry while preserving translational symmetry, exist in several families of unconventional superconductors. Superconductivity mediated by nematic fluctuations is well established theoretically, but it has yet to be unambiguously identified experimentally. One major challenge is that nematicity is often intertwined with other degrees of freedom, such as magnetism and charge order. The FeSe1-xSx family of superconductors provides an opportunity to explore this concept, as it features an isolated nematic phase that can be suppressed by sulfur substitution at a quantum critical point where the nematic fluctuations are the largest. Here we determine the momentum structure of the superconducting gap near the centre of the Brillouin zone in FeSe0.81S0.19-close to the quantum critical point-and find that it is anisotropic and nearly nodal. The gap minima occur in a direction that is rotated 45 degrees with respect to the Fe-Fe direction, unlike the usual isotropic gaps due to spin-mediated pairing in other tetragonal Fe-based superconductors. Instead, we find that the gap structure agrees with theoretical predictions for superconductivity mediated by nematic fluctuations, indicating a change in the pairing mechanism across the phase diagram of FeSe1--xSx. Superconductivity that is mediated by fluctuations of a nematic electronic order has not been experimentally demonstrated. Now an analysis of the symmetry of the superconducting gap in doped FeSe provides evidence of this phenomenon.

NATURE PHYSICS, 2024. DOI: 10.1038/s41567-024-02683-x Early Access Date: NOV 2024

[P250-2024] "Highly Efficient Compact Acousto-Optic Modulator Based on a Hybrid-Lattice Hollow Core Fiber"

Silva, R. E. da*; Osório, J. H.; Webb, D. J.; Gérôme, F.; Benabid, F.; Franco, M. A. R.; **Cordeiro, C. M. B.***

We demonstrate the acousto-optic modulation of a hybrid--lattice hollow core fiber (HL-HCF) for the first time. For many years, optical fibers with reduced diameters have been the main solution to increase the interaction of acoustic and optical waves. However, the high drive voltages and large modulator components still employed drastically affect the efficiency and miniaturization of these devices. Here, we experimentally show that combining Kagom & eacute; and tubular lattices in HL-HCFs allows for enhancing the amplification of the acoustic waves and the modulation of the guided optical modes, thus providing high modulation efficiency even when using a fiber with a 240 mu m diameter. To the best of our knowledge, the measured HL-HCF's modulation efficiency (1.3 dB/V) is the highest compared to devices employing reduced diameter fibers. Additionally, we demonstrate a compact acousto-optic modulator with driver dimensions smaller than the HL-HCF diameter. Overall, our results show a promising alternative to solve the compromise of speed, efficiency, and compactness for integration with microscale all-fiber photonic devices.

IEEE PHOTONICS TECHNOLOGY LETTERS 36[24], 1441-1444, 2024. DOI: 10.1109/LPT.2024.3487478

[P251-2024] "In-situ transmission electron microscopy (TEM) investigation of the reduction process in graphene oxide"

Silva, D. S. da*; Viana, G. A.*; Silva Filho, J. M. C. da*; Kretly, L. C.; Neto, A. M. J. C.; Vieira, L.; Barros, T. A. S.; **Marques, F. C.***

The reduction processes of graphene oxide (GO) aim to remove functional groups such as H2O, CO, and CO2 to promote the properties of GO towards those of pure graphene. We adopted the thermal reduction process from room temperature to 320 degrees C. The transmission electron microscopy (TEM) technique was used to probe the effect of reduction mechanisms. It was observed that the plasmon peaks, referring to sp2 carbon bonds in crystalline structures, are more evident in the reduced graphene oxide (rGO) than GO. The fine structure at the K edge of carbon shows differences in shape linked to the density of states above the Fermi level. Electron energy loss spectroscopy (EELS) analyses revealed an increase in the fraction of sp3 bonds in the reduced sample, consistent with the reduction of functional radicals in the GO structure.

MRS ADVANCES, 2024. DOI: 10.1557/s43580-024-00998-8 Early Access Date: NOV 2024

[P252-2024] "Inclusive and differential cross section measurements of t(t)over-barb (b)over-bar production in the lepton plus jets channel at √s=13 TeV"

Hayrapetyan, A.; Tumasyan, A.; Adam, W.; **Chinellato, J. A.***; et al.
CMS Collaboration

Measurements of inclusive and normalized differential cross sections of the associated production of top quark-antiquark and bottom quark-antiquark pairs, t (t) over barb (b) over bar, are presented. The results are based on data from proton--proton collisions collected by the CMS detector at a centre--of-mass energy of 13TeV, corresponding to an integrated luminosity of 138 fb(-1). The cross sections are measured in the lepton+jets decay channel of the top quark pair, using events containing exactly one isolated electron or muon and at least five jets. Measurements are made in four fiducial phase space regions, targeting different aspects of the t (t) over barb (b) over bar b process. Distributions are unfolded to the particle level through maximum likelihood fits, and compared with predictions from several event generators. The inclusive cross section measurements of this process in the fiducial phase space regions are the most precise to date. In most cases, the measured inclusive cross sections exceed the predictions with the chosen generator settings. The only exception is when using a particular choice of dynamic renormalization scale, mu R = 1/2 pi(i=t), (t) over bar t,b,(b) over bar m(1/4) (T, i,) where m(T)(2), i = m(i)(2) + p(T,i)(2) are the transverse masses of top and bottom quarks. The differential cross sections show varying degrees of compatibility with the theoretical predictions, and none of the tested generators with the chosen settings simultaneously describe all the measured distributions.

JOURNAL OF HIGH ENERGY PHYSICS [5], 042, 2024. DOI: 10.1007/JHEP05(2024)042

[P253-2024] "Infrared properties of the quark-gluon vertex in general kinematics"

Aguilar, A. C.*; Ferreira, M. N.; **Oliveira, B. M.***; Papavassiliou, J. ; **Teixeira, G. L.***

In the present work we determine the eight form factors of the transversely-projected quark-gluon vertex in general kinematics, in the context of Landau-gauge QCD with two degenerate light dynamical quarks. The study is based on the set of Schwinger-Dyson equations that govern the vertex form factors, derived within the formalism of the three-particle--irreducible (3PI) effective action. The analysis is performed by employing lattice data for the main ingredients, such as gluon and quark propagators, and three-gluon vertex. The numerical treatment is simplified by decoupling the system of integral equations: the classical form factor is determined from a single non-linear equation involving only itself, while the remaining ones are subsequently computed through simple integrations. The form factors are obtained for arbitrary values of space-like momenta, and their angular dependence is examined in detail. A clear hierarchy is established at the level of the corresponding dimensionless effective couplings, in agreement with results of earlier studies. Furthermore, the classical form factor is found to be in excellent agreement with recent unquenched lattice data in the soft-gluon configuration, while the two non-classical dressings depart substantially from the lattice results. Finally, the accurate implementation of multiplicative renormalizability is confirmed, and the transition from Minkoswski to Euclidean space is elucidated.

EUROPEAN PHYSICAL JOURNAL C 84[11], 1231, 2024. DOI: 10.1140/epjc/s10052-024-13605-9

[P254-2024] "Isostructural Oxamate Complexes with Visible Luminescence" (Eu3+) and Field-Induced Single-Molecule Magnet (Nd3+)"

Diogo, E. B. T.; Silva Jr., E. N. da; Oliveira, W. X. C.; Stumpf, H. O.; **Fabris, F.*; Almeida, A. A. de*; Knobel, M.***; Ferreira, F. F.; Nunes, W. C.; Pedroso, E. F.; Julve, M.; Pereira, C. L. M.

The search for new metal-organic compounds as candidates for quantum information processing technologies is in the spotlight. Several metal ions and organic linkers have been used to obtain such compounds. Herein, we describe the synthesis, crystal structures, and cryomagnetic properties of two air-stable isostructural neodymium(III) and europium(III) one-dimensional (1D) coordination polymers of formula [Nd(Hmpa)3(DMSO)2]n (1) and [Eu(Hmpa)3(DMSO)2]n (2) [Hmpa=N-(4-methylphenyl) oxamate, and DMSO=dimethylsulfoxide]. These complexes were prepared by reacting n-Bu4N(Hmpa) proligand [n--Bu4N+=tetra-n-butylammonium] and the correspondent LnCl3 & sdot; 6H2O salt (Ln=Nd or Eu) in the open air and mild conditions. The crystal structures of 1 and 2 reveal the Ln3+ ion surrounded by two DMSO molecules and three oxamate ligands, one of them connecting to adjacent mononuclear entities through carboxylate bridges featuring a homometallic chain, while the other two establishing double N-H & sdot; & sdot; & sdot; O hydrogen bonds among adjacent polymers to give a resultant supramolecular 2D network. Cryomagnetic measurements in the static (dc) and dynamic current (ac) regimes reveal that 1 behaves as a field-induced single-molecule magnet below 8.8 K. A photoluminescence study shows that Hmpa ligands efficiently sensitize the luminescence of Eu3+ complex in the visible region in the solid state at room temperature.

CHEMISTRY-AN ASIAN JOURNAL, 2024. DOI: 10.1002/asia.202400887 Early Access Date: OCT 2024

[P255-2024] "Lattice determination of the Batalin-Vilkovisky function and the strong running interaction"

Aguilar, A. C.*; Brito, N.; Ferreira, M. N.; Papavassiliou, J.; Oliveira, O.; Silva, P. J.

The Batalin-Vilkovisky function is a central component in the modern formulation of the background field method and the physical applications derived from it. In the present work we report on novel lattice results for this particular quantity, obtained by capitalizing on its equality with the Kugo-Ojima function in the Landau gauge. The results of the lattice simulation are in very good agreement with the predictions derived from a continuum analysis based on the corresponding Schwinger-Dyson equations. In addition, we show that an important relation connecting this function with the ghost propagator is fulfilled rather accurately. With the aid of these results, we carry out the first completely lattice-based determination of the process-independent strong running interaction, employed in a variety of phenomenological studies.

PHYSICS LETTERS B 858, 139054, 2024. DOI: 10.1016/j.physletb.2024.139054

[P256-2024] "Light-flavor particle production in high-multiplicity pp collisions at √s=13 TeV as a function of transverse spherocity"

Acharya, S.; Adamova, D.; Rinella, G. A.; **Chinellato, D. D.*; Guardiano, G. G.*; Liveraro, G. S. S.*; Takahashi, J.*;** et al. ALICE Collaboration

Results on the transverse spherocity dependence of light-flavor particle production (pi, K, p,phi, K-*0, K-S(0),Lambda.,Xi) at midrapidity in high-multiplicity pp collisions at root s = 13TeV were obtained with the ALICE apparatus. The transverse spherocity estimator (S-O(pT)=1) categorizes events by their azimuthal topology. Utilizing narrow selections on S-O(pT)=1, it is possible to contrast particle production in collisions dominated by many soft initial interactions with that observed in collisions dominated by one or more hard scatterings. Results are reported for two multiplicity estimators covering different pseudorapidity regions. The S-O(pT-1) estimator is found to effectively constrain the hardness of the events when the midrapidity (|eta| < 0.8) estimator is used. The production rates of strange particles are found to be slightly higher for soft isotropic topologies, and severely suppressed in hard jet--like topologies. These effects are more pronounced for hadrons with larger mass and strangeness content, and observed when the topological selection is done within a narrow multiplicity interval. This demonstrates that an important aspect of the universal scaling of strangeness enhancement with final-state multiplicity is that high-multiplicity collisions are dominated by soft, isotropic processes. On the contrary, strangeness production in events with jet-like processes is significantly reduced. The results presented in this article are compared with several QCD-inspired Monte Carlo event generators. Models that incorporate a two-component phenomenology, either through mechanisms accounting for string density, or thermal production, are able to describe the observed strangeness enhancement as a function of S-O(pT=1) .

JOURNAL OF HIGH ENERGY PHYSICS [5], 184, 2024. DOI: 10.1007/JHEP05(2024)184

[P257-2024] "Machine Learning Applied to Terahertz Signal Analysis for Hygrothermal Aging Characterization of Composites"

Marinho, C. A.; Silva, A. H. da; Ferreira, C. G.; Cardoso, D. C. T.; Lopes, B. J.; **Netto, G. B.*; Siqueira, J. P.*; Cruz, F. C.***; Junior, M. V. B.

Given their noncontact nature, ease of inspecting nonmetallic materials, and ability to detect small structural changes, terahertz waves were chosen as the study methodology for this project. Initially, characterization data was pretreated and standardized. The data were then reduced in dimensionality using principal component analysis and classified using other machine learning methods. The results demonstrated that the terahertz wave technique could accurately distinguish between different temperature and aging time scenarios. They also indicated that nondestructive in-service characterization of composite repairs is feasible and can provide invaluable information for decision-making. The main benefits of this approach include ensuring the safe operation of offshore piping and optimizing resources when deciding whether to replace the repair or keep it in service. KEYWORDS: terahertz nondestructive evaluation, machine learning characterization, composite repairs, glass fiber reinforced polymer (GFRP).

MATERIALS EVALUATION 82[8], 2024. DOI: 10.32548/2024.me-04425

[P258-2024] "Measurement of inclusive charged-particle jet production in pp and p-Pb collisions at √sNN=5.02 TeV"

Acharya, S.; Adamová, D.; Adler, A.; **Chinellato, D. D.*; Guardiano, G. G.*; Jahnke, C.*; Liveraro, G. S. S.*; Takahashi, J.***; et al.
ALICE Collaboration

Measurements of inclusive charged-particle jet production in pp and p-Pb collisions at center-of-mass energy per nucleon--nucleon collision root s(NN) = 5.02TeV and the corresponding nuclear modification factor R-pPb(ch jet) are presented, using data collected with the ALICE detector at the LHC. Jets are reconstructed in the central rapidity region |eta(jet)| < 0.5 from charged particles using the anti-k(T) algorithm with resolution parameters R = 0.2, 0.3, and 0.4. The p(T)-differential inclusive production cross section of charged-particle jets, as well as the corresponding cross section ratios, are reported for pp and p-Pb collisions in the transverse momentum range 10 < p(T,jet)(ch) < 140 GeV/ c and 10 < p(T,jet)(ch) < 160 GeV/c, respectively, together with the nuclear modification factor R-pPb(ch jet) in the range 10 < p(T,jet)(ch) < 140 GeV/c. The analysis extends the p(T) range of the previously-reported charged-particle jet measurements by the ALICE Collaboration. The nuclear modification factor is found to be consistent with one and independent of the jet resolution parameter with the improved precision of this study, indicating that the possible influence of cold nuclear matter effects on the production cross section of charged-particle jets in p-Pb collisions at root s(NN) = 5.02TeV is smaller than the current precision. The obtained results are in agreement with other minimum bias jet measurements available for RHIC and LHC energies, and are well reproduced by the NLO perturbative QCD Powheg calculations with parton shower provided by Pythia8 as well as by Jetscape simulations.

JOURNAL OF HIGH ENERGY PHYSICS [5], 041, 2024. DOI: 10.1007/JHEP05(2024)041

[P259-2024] "Measurement of simplified template cross sections of the Higgs boson produced in association with W or Z bosons in the H -- bb decay channel in proton-proton collisions at √s=13 TeV"

Tumasyan, A.; Adam, W.; Andrejkovic, J. W.; **Chinellato, J. A.*;** et al.
CMS Collaboration

Differential cross sections are measured for the standard model Higgs boson produced in association with vector bosons (W, Z) and decaying to a pair of b quarks. Measurements are performed within the framework of the simplified template cross sections. The analysis relies on the leptonic decays of theW and Z bosons, resulting in final states with 0, 1, or 2 electrons or muons. The Higgs boson candidates are either reconstructed from pairs of resolved b--tagged jets, or from single large-radius jets containing the particles arising from two b quarks. Proton-proton collision data at root s = 13 TeV, collected by the CMS experiment in 2016-2018 and corresponding to a total integrated luminosity of 138 fb(-1), are analyzed. The inclusive signal strength, defined as the product of the observed production cross section and branching fraction relative to the standard model expectation, combining all analysis categories, is found to be mu = 1.15(-0.20)(+0.22). This corresponds to an observed (expected) significance of 6.3 (5.6) standard deviations.

PHYSICAL REVIEW D 109[9], 092011, 2024. DOI: 10.1103/PhysRevD.109.092011

[P260-2024] "Measurement of the absolute efficiency of the X-ARAPUCA photon detector for the DUNE Far Detector 1"

Alvarez-Garrote, R.; Brizzolari, C.; Canto, A.; Calvo, E.; Cattadori, C. M.; Cuesta, C.; Rojo, A. de la Torre; Gil-Botella, I.; Gotti, C.; Guffanti, D.; **Machado, A. A.***; Corchado, S. Manthey; Martin, I.; Massari, C.; Meazza, L.; Palomares, C.; Perez--Molina, L.; Segreto, E.; Terranova, F.; Osa, A. Verdugo de; Souza, H. V. de; Warner, D.

The DUNE far detector has been designed to detect photons and electrons generated by the charged products of the interaction of neutrinos with a massive liquid argon (LAr) target. The photon detection system (PDS) of the first DUNE far detector (FD1) is composed of 6000 photon detection units, named X-ARAPUCA. The detection of the prompt light pulse generated by the particle energy release in LAr will complement and boost the DUNE LAr Time Projection Chamber. It will improve the non-beam events tagging and enable at low energies the trigger and the calorimetry of the supernova neutrinos. The X-ARAPUCA is an assembly of several components. Its photon detection efficiency (PDE) depends on the design of the assembly, on the grade of the individual components and on their coupling. The X-ARAPUCA PDE is one of the leading parameters for the PDS sensitivity, that in turn determines the sensitivity of the DUNE for the detection of core-collapse supernova within the galaxy and for nucleon decay searches. In this work we present the final assessment of the absolute PDE of the FD1 X-ARAPUCA baseline design, measured in two laboratories with independent methods and setups. Preliminary results were reported in Palomares (JINST 18(02):C02064, https://doi.org/10.1088/1748-0221/18/02/C02064, 2023). One hundred sixty units of these X-ARAPUCA devices have been deployed in the NP04 facility at the CERN Neutrino Platform, the 1:20 scale FD1 prototype, and will be operated during the year 2024. The assessed value of the PDE is a key parameter both in the NP04 and in the DUNE analysis and reconstruction studies.

EUROPEAN PHYSICAL JOURNAL C 84[10], 1004, 2024. DOI: 10.1140/epjc/s10052-024-13393-2

[P261-2024] "Measurement of the primary Lund jet plane density in proton-proton collisions at √s=13 TeV"

Hayrapetyan, A.; Tumasyan, A.; Adam, W.; **Chinellato, J. A.***; et al.
CMS Collaboration

A measurement is presented of the primary Lund jet plane (LJP) density in inclusive jet production in proton--proton collisions. The analysis uses 138 fb(-1) of data collected by the CMS experiment at root s = 13TeV.

The LJP, a representation of the phase space of emissions inside jets, is constructed using iterative jet declustering. The transverse momentum kT and the splitting angle Delta R of an emission relative to its emitter are measured at each step of the jet declustering process. The average density of emissions as function of ln(k(T)/GeV) and ln(R/Delta R) is measured for jets with distance parameters R = 0.4 or 0.8, transverse momentum p(T) > 700 GeV, and rapidity |y| < 1.7. The jet substructure is measured using the charged-particle tracks of the jet. The measured distributions, unfolded to the level of stable charged particles, are compared with theoretical predictions from simulations and with perturbative quantum chromodynamics calculations. Due to the ability of the LJP to factorize physical effects, these measurements can be used to improve different aspects of the physics modeling in event generators.

JOURNAL OF HIGH ENERGY PHYSICS [5], 116, 2024. DOI: 10.1007/JHEP05(2024)116

[P262-2024] "Measurements of Chemical Potentials in Pb-Pb Collisions at √sNN=5.02 TeV"

Acharya, S.; Adamova, D.; **Chinellato, D. D.*; Guardiano, G. G.*; Liveraro, G. S. S.*; Takahashi, J.***; et al.
ALICE Collaboration

This Letter presents the most precise measurement to date of the matter-antimatter imbalance at midrapidity in Pb-Pb collisions at a center-of-mass energy per nucleon pair root s(NN) = 5.02 TeV. Using the Statistical Hadronization framework, it is possible to obtain the value of the electric charge and baryon chemical potentials, mu(Q) = -0.18 +/- 0.90 MeV and mu(B) = 0.71 +/- 0.45 MeV, with unprecedented precision. A centrality-differential study of the antiparticle-to-particle yield ratios of charged pions, protons, Omega baryons, and light (hyper)nuclei is performed. These results indicate that the system created in Pb-Pb collisions at the LHC is on average baryon-free and electrically neutral at midrapidity.

PHYSICAL REVIEW LETTERS 133[9], 092301, 2024. DOI: 10.1103/PhysRevLett.133.092301

[P263-2024] "Measurements of jet quenching using semi-inclusive hadron plus jet distributions in pp and central Pb-Pb collisions at √sNN=5.02 TeV"

Acharya, S.; Adamova, D.; Rinella, G. A.; **Chinellato, D. D.*; Guardiano, G. G.*; Liveraro, G. S. S.*; Takahashi, J.***; et al.
ALICE Collaboration

The ALICE Collaboration reports measurements of the semi-inclusive distribution of charged-particle jets recoiling from a high transverse momentum (high p(T)) charged hadron, in pp and central Pb-Pb collisions at center-of-mass energy per nucleon-nucleon collision root s(NN) = 5.02 TeV. The large uncorrelated background in central Pb-Pb collisions is corrected using a data-driven statistical approach which enables precise measurement of recoil jet distributions over a broad range in p(T,ch jet) and jet resolution parameter R. Recoil jet yields are reported for R = 0.2, 0.4, and 0.5 in the range 7 < p(T,ch jet) < 140 GeV/c and pi/2 < Delta phi < pi, where Delta phi is the azimuthal angular separation between hadron trigger and recoil jet. The low-p(T,ch jet) reach of the measurement explores unique phase space for studying jet quenching, the interaction of jets with the quark-gluon plasma generated in high-energy nuclear collisions. Comparison of p(T,ch jet) distributions from pp and central Pb-Pb collisions probes medium-induced jet energy loss and intra-jet broadening, while comparison of their acoplanarity distributions explores in-medium jet scattering and medium response. The measurements are compared to theoretical calculations incorporating jet quenching.

PHYSICAL REVIEW C 110[1], 014906, 2024. DOI: 10.1103/PhysRevC.110.014906

[P264-2024]"Multiplicity-dependent production of Σ(1385)± and (1530)0 in pp collisions at √s=13 TeV"

Acharya, S.; Adamova, D.; Rinella, G. A.; **Chinellato, D. D.*; Guardiano, G. G.*; Jahnke, C.*; Liveraro, G. S. S.*; Takahashi, J.***; et al.
ALICE Collaboration

The production yields of the Sigma(1385)(+/-) and.(1530)(0) resonances are measured in pp collisions at root s = 13TeV with ALICE. The measurements are performed as a function of the charged-particle multiplicity dN(ch)/d eta , which is related to the energy density produced in the collision. The results include transverse momentum (p(T)) distributions, p(T)-integrated yields, mean transverse momenta of Sigma(1385)(+/-) and.(1530)(0), as well as ratios of the p(T)-integrated resonance yields relative to yields of other hadron species. The Sigma(1385)(+/-)/pi(+/-) and Xi(1530)(0)/ pi(+/-) yield ratios are consistent with the trend of the enhancement of strangeness production from low to high multiplicity pp collisions, which was previously observed for strange and multi-strange baryons. The yield ratio between the measured resonances and the long-lived baryons with the same strangeness content exhibits a hint of a mild increasing trend at low multiplicity, despite too large uncertainties to exclude the flat behaviour. The results are compared with predictions from models such as EPOS-LHC and PYTHIA 8 with Rope shoving. The latter provides the best description of the multiplicity dependence of the Sigma(1385)(+/-) and Xi(1530)(0) production in pp collisions at root s = 13TeV.

JOURNAL OF HIGH ENERGY PHYSICS [5], 317, 2024. DOI: 10.1007/JHEP05(2024)317

[P265-2024] "N-acetylcysteine effects on extracellular polymeric substances of Xylella fastidiosa: A spatiotemporal investigation with implications for biofilm disruption"

Silva, A. M. da*; Murillo, D. M.*; Anbumani, S.*; von Zuben, A. A.*; Cavalli, A.; **Obata, H. T.***; Fischer, E. R.; Souza e Silva, M. de; Bakkers, E.; Souza, A. A.; Carvalho, H. F.; **Cotta, M. A.***

Background: The matrix of extracellular polymeric substances (EPS) present in biofilms greatly amplifies the problem of bacterial infections, protecting bacteria against antimicrobial treatments and eventually leading to bacterial resistance. The need for alternative treatments that destroy the EPS matrix becomes evident. N-acetylcysteine (NAC) is one option that presents diverse effects against bacteria; however, the different mechanisms of action of NAC in biofilms have yet to be elucidated. Objectives: In this work, we performed microscopy studies at micro and nano scales to address the effects of NAC at single cell level and early-stage biofilms of the Xylella fastidiosa phytopathogen. Methods: We show the physical effects of NAC on the adhesion surface and the different types of EPS, as well as the mechanical response of individual bacteria to NAC concentrations between 2 and 20 mg/mL. Results: NAC modified the conditioning film on the substrate, broke down the soluble EPS, resulting in the release of adherent bacteria, decreased the volume of loosely bound EPS, and disrupted the biofilm matrix. Tightly bound EPS suffered structural alterations despite no solid evidence of its removal. In addition, bacterial force measurements upon NAC action performed with InP nanowire arrays showed an enhanced momentum transfer to the nanowires due to increased cell mobility resulting from EPS removal. Conclusions: Our results clearly show that conditioning film and soluble EPS play a key role in cell adhesion control and that NAC alters EPS structure, providing solid evidence that NAC actuates mainly on EPS removal, both at single cell and biofilm levels.

INTERNATIONAL JOURNAL OF ANTIMICROBIAL AGENTS 64[5], 107340, 2024. DOI: 10.1016/j.ijantimicag.2024.107340

[P266-2024] "Neuromuscular characteristics of eccentric, concentric and isometric contractions of the knee extensors"

Ruas, C. V.*; Taylor, J. L.; Latella, C.; Haff, G. G.; Nosaka, K.

Purpose We compared voluntary drive and corticospinal responses during eccentric (ECC), isometric (ISOM) and concentric (CON) muscle contractions to shed light on neurophysiological mechanisms underpinning the lower voluntary drive in a greater force production in ECC than other contractions. Methods Sixteen participants (20-33 years) performed ISOM and isokinetic (30 degrees/s) CON and ECC knee extensor contractions (110 degrees-40 degrees knee flexion) in which electromyographic activity (EMG) was recorded from vastus lateralis. Voluntary activation (VA) was measured during ISOM, CON and ECC maximal voluntary contractions (MVCs). Transcranial magnetic stimulation elicited motor-evoked potentials (MEPs) and corticospinal silent periods (CSP) during MVCs and submaximal (30%) contractions, and short-interval intracortical inhibition (SICI) in submaximal contractions. Results MVC torque was greater (P < 0.01) during ECC (302.6 +/- 90.0 Nm) than ISOM (269.8 +/- 81.5 Nm) and CON (235.4 +/- 78.6 Nm), but VA was lower (P < 0.01) for ECC (68.4 +/- 14.9%) than ISOM (78.3 +/- 13.1%) and CON (80.7 +/- 15.4%). In addition, EMG/torque was lower (P < 0.02) for ECC (1.9 +/- 1.1 mu V(.)Nm(-1)) than ISOM (2.2 +/- 1.2 mu V.Nm(-1)) and CON (2.7 +/- 1.6 mu V(.)Nm(-1)), CSP was shorter (p < 0.04) for ECC (0.097 +/- 0.03 s) than ISOM (0.109 +/- 0.02 s) and CON (0.109 +/- 0.03 s), and MEP amplitude was lower (P < 0.01) for ECC (3.46 +/- 1.67 mV) than ISOM (4.21 +/- 2.33 mV) and CON (4.01 +/- 2.06 mV). Similar results were found for EMG/torque and CSP during 30% contractions, but MEP and SICI showed no differences among contractions (p > 0.05). Conclusions The lower voluntary drive indicated by reduced VA during ECC may be partly explained by lower corticospinal excitability, while the shorter CSP may reflect extra muscle spindle excitation of the motoneurons from vastus lateralis muscle lengthening.

EUROPEAN JOURNAL OF APPLIED PHYSIOLOGY, 2024. DOI: 10.1007/s00421-024-05626-9

[P267-2024] "Non-thermal magnetic deicing using two-dimensional chromium telluride"

Gowda, C. C.; Kartsev, A.; Tiwari, N.; Safronov, A. A.; Pandey, P.; Roy, A. K.; Ajayan, P. M.; **Galvao, D. S.***; Tiwary, C. S.

Two-dimensional (2D) chromium telluride Cr2Te3 exhibits strong ferromagnetic ordering with high coercivity at low temperatures and paramagnetic behavior when approaching room temperature. The spin states of monolayer Cr2Te3 show ferromagnetic ordering in the ground state. In situ Raman analysis reveals a reversible structure transformation and hence proves ferromagnetic to paramagnetic transition during low-temperature heating cycles (0-25 degrees C). The magnetic phase transition near room temperature in 2D Cr2Te3 prompted an exploratory study of these layered materials for energy application. We demonstrate that the low-temperature ferromagnetic behavior can be used to magnetically deice material surfaces using an external magnetic source, avoiding the use of harsh chemicals and high temperatures. The hydrophobic nature and dipole interactions of H2O molecules with the surface of the 2D Cr2Te3 coating aid in the condensation of ice droplets formed on the surfaces. First-principles calculations also confirm the observed crystal structure, surface interaction, and magnetic properties of 2D Cr2Te3. Icing of surfaces is a major issue that affects the livelihood of people residing in the northern hemisphereThis study focuses on deicing of surfaces with materials exhibiting near room temperature ferromagnetism.

JOURNAL OF MATERIALS CHEMISTRY C, 2024. DOI: 10.1039/d4tc02542c. Early Access Date: OCT 2024

[P268-2024] "Nonperturbative four-gluon vertex in soft kinematics"

Aguilar, A. C.*; De Soto, F.; Ferreira, M. N.; Papavassiliou, J.; Pinto-Gomez, F.; Rodriguez-Quintero, J.; **Santos, L. R.***

We present a nonperturbative study of the form factor associated with the projection of the full four-gluon vertex on its classical tensor, for a set of kinematics with one vanishing and three arbitrary external momenta. The treatment is based on the Schwinger-Dyson equation governing this vertex, and a large-volume lattice simulation, involving ten thousand gauge field configurations. The key hypothesis employed in both approaches is the "planar degeneracy", which classifies diverse configurations by means of a single variable, thus enabling their meaningful "averaging". The results of both approaches show notable agreement, revealing a considerable suppression of the averaged form factor in the infrared. The deviations from the exact planar degeneracy are discussed in detail, and a supplementary variable is used to achieve a more accurate description. The effective charge defined through this special form factor is computed within both approaches, and the results obtained are in excellent agreement.

PHYSICS LETTERS B 858, 139065, 2024. DOI: 10.1016/j.physletb.2024.139065

[P269-2024]"Nonresonant central exclusive production of charged-hadron pairs in proton-proton collisions at √s=13 TeV"

Hayrapetyan, A.; Tumasyan, A.; Adam, W.; **Chinellato, J. A.***; et al.
CMS Collaboration; TOTEM Collaboration

The central exclusive production of charged-hadron pairs in pp collisions at a center-of-mass energy of 13 TeV is examined, based on data collected in a special high-beta* run of the LHC. The nonresonant continuum processes are studied with the invariant mass of the centrally produced twopion system in the resonance-free region, m(pi+pi-) < 0.7 or m(pi+pi-) > 1.8 GeV. Differential cross sections as functions of the azimuthal angle between the surviving protons, squared exchanged four- momenta, and m(pi+pi-) are measured in a wide region of scattered proton transverse momenta, between 0.2 and 0.8 GeV, and for pion rapidities |y| < 2. A rich structure of interactions related to double-pomeron exchange is observed. A parabolic minimum in the distribution of the two-proton azimuthal angle is observed for the first time. It can be interpreted as an effect of additional pomeron exchanges between the protons from the interference between the bare and the rescattered amplitudes. After model tuning, various physical quantities are determined that are related to the pomeron cross section, protonpomeron and meson-pomeron form factors, pomeron trajectory and intercept, and coefficients of diffractive eigenstates of the proton.

PHYSICAL REVIEW D 109[11], 112013, 2024. DOI: 10.1103/PhysRevD.109.112013

[P270-2024] "Nuclear compensatory evolution driven by mito-nuclear incompatibilities"

Princepe, D.*; Aguiar, M. A. M. de*

Mitochondrial function relies on the coordinated expression of mitochondrial and nuclear genes, exhibiting remarkable resilience despite high mitochondrial mutation rates.

The nuclear compensation mechanism suggests deleterious mitochondrial alleles drive compensatory nuclear mutations to preserve mito-nuclear compatibility. However, prevalence and factors conditioning this phenomenon remain debated due to its conflicting evidence. Here, we investigate how mito--nuclear incompatibilities impact substitutions in a model for species radiation. Mating success depends on genetic compatibility (nuclear DNA) and spatial proximity. Populations evolve from partially sion. Mutations do not confer advantages nor disadvantages, but individual fecundity declines with increasing incompatibilities, selecting for mito-nuclear coordination. We find that selection for mito-nuclear compatibility affects each genome differently based on their initial state. In compatible gene pairs, selection reduces substitutions in both genomes, while in incompatible nuclear genes, it consistently promotes compensation, facilitated by more mismatches. Interestingly, high mitochondrial mutation rates can reduce nuclear compensation by increasing mtDNA rectification, while substitutions in initially compatible nuclear gene are boosted. Finally, the presence of incompatibilities accelerates species radiation, but equilibrium richness is not directly correlated to substitution rates, revealing the complex dynamics triggered by mitochondrial introgression and mito-nuclear coevolution. Our study provides a perspective on nuclear compensation and the role of mito-nuclear incompatibilities in speciation by exploring extreme scenarios and identifying trends that empirical data alone cannot reveal. We emphasize the challenges in detecting these dynamics and propose analyzing specific genomic signatures could shed light on this evolutionary process.

PROCEEDINGS OF THE NATIONAL ACADEMY OF SCIENCES OF THE UNITED STATES OF AMERICA 121[42], e2411672121, 2024. DOI: 10.1073/pnas.2411672121

[P271-2024] "Observation of the Ξb- -- ψ(2S)Ξ- decay and studies of the Ξb (5945)0 baryon in proton-proton collisions at √s=13 TeV"

Hayrapetyan, A.; Tumasyan, A.; Adam, W.; **Chinellato, J. A.***; et al.
CMS Collaboration

The first observation of the decay Xi(-)(b) -> psi(2S)Xi(-) and measurement of the branching ratio of Xi(-)(b) -> psi(2S)Xi(-) to Xi(-)(b) -> J/psi Xi(-) are presented. The J/psi and psi(2S) mesons are reconstructed using their dimuon decay modes. The results are based on proton-proton colliding beam data from the LHC collected by the CMS experiment at root s = 13 TeV in 2016-2018, corresponding to an integrated luminosity of 140 fb(-1). The branching fraction ratio is measured to be B(Xi(-)(b) -> psi(2S)Xi(-))/B(Xi(-)(b) -> J/psi Xi(-)) = 0.84(-0.19)(+0.21) (stat) +/- 0.10(syst) +/- 0.02(B), where the last uncertainty comes from the uncertainties in the branching fractions of the charmonium states. New measurements of the Xi(b) (5945)(0) baryon mass and natural width are also presented, using the Xi(-)(b)pi(+) final state, where the Xi(-)(b) baryon is reconstructed through the decays J/psi Xi(-), psi(2S)Xi(-), J/psi Lambda K-, and J/psi Sigma K-0(-). Finally, the fraction of Xi(-)(b) baryons produced from Xi(b) (5945)(0) decays is determined.

PHYSICAL REVIEW C 110[1], 012002, 2024. DOI: 10.1103/PhysRevD.110.012002

[P272-2024] "Observation of the γ(3S) Meson and Suppression of γ States in Pb-Pb Collisions at √sNN=5.02 TeV"

Tumasyan, A.; Adam, W.; Andrejkovic, J. W.; **Chinellato, J. A.***; et al. CMS Collaboration

The production of gamma(2S) and gamma(3S) mesons in lead--lead (Pb-Pb) and proton-proton (pp) collisions is studied in their dimuon decay channel using the CMS detector at the LHC. The gamma(3S) meson is observed for the first time in Pb-Pb collisions, with a significance above 5 standard deviations. The ratios of yields measured in Pb-Pb and pp collisions are reported for both the gamma(2S) and gamma(3S) mesons, as functions of transverse momentum and Pb-Pb collision centrality. These ratios, when appropriately scaled, are significantly less than unity, indicating a suppression of gamma yields in Pb-Pb collisions. This suppression increases from peripheral to central Pb-Pb collisions. Furthermore, the suppression is stronger for gamma(3S) mesons compared to gamma(2S) mesons, extending the pattern of sequential suppression of quarkonium states in nuclear collisions previously seen for the J/psi, psi(2S), gamma(1S), and gamma(2S) mesons.

PHYSICAL REVIEW LETTERS 133[2], 022302, 2024. DOI: 10.1103/PhysRevLett.133.022302

[P273-2024] "Observational-interventional Bell inequalities"

Poderini, D.; Nery, R.; Moreno, G.; Zamora, S.; **Lauand, P.***; Chaves, R.

Generalizations of Bell's theorem, particularly within quantum networks, are now being analyzed through the lens of causal inference. However, the exploration of interventions, a central concept in causality theory, remains significantly unexplored. In this work, we take an initial step in this direction, by analyzing the instrumental scenario and proposing hybrid Bell inequalities integrating observational and interventional data. Focusing on binary outcomes with any number of inputs, we obtain the complete characterization of the observational-interventional polytope, equivalent to a Hardy-like Bell inequality, albeit describing a distinct quantum experiment. To illustrate its applications, we show a significant enhancement regarding threshold detection efficiencies for quantum violations also showing the use of this hybrid approach in quantum steering scenarios.

PHYSICAL REVIEW A 110[4], 042213, 2024. DOI: 10.1103/PhysRevA.110.042213

[P274-2024] "On the Non-Catalytic Role of Lytic Polysaccharide Monooxygenases in Boosting the Action of PETases on PET Polymers"

Corrêa, T. L. R.; Román, E. K. B.; Costa, C. A. R.; Wolf, L. D.; **Landers, R.***; Biely, P.; Murakami, M. T.; Walton, P. H.

Synthetic polymers are resistant to biological attack, resulting in their long-term accumulation in landfills and in natural aquatic and terrestrial habitats. Lytic polysaccharide monooxygenases (LPMOs) are enzymes which oxidatively cleave the polysaccharide chains in recalcitrant polysaccharides such as cellulose. It has been widely hypothesised that LPMOs could be used to aid in the enzymatic breakdown of synthetic polymers. Herein, through the use of biochemical assays, X-ray photoelectron spectroscopy (XPS) and atomic force microscopy (AFM) we show that LPMOs can bind to polyethylene terephthalate (PET), and - in doing so - the hydrophobic surface of PET becomes more hydrophilic such that product release is boosted by subsequent treatment with classical PETases. The boosting effect is however, only observed in reactions when the LPMO and the PETase are added sequentially rather than simultaneously to the PET. Moreover, the same boosting effect is also seen when a catalytically-inactive mutant of LPMO is used, showing that the principal means by which AA9 LPMOs boost the degradation of synthetic polymers is through their role as a "hydrophobin" rather than as an oxygenase. Indeed, in accord with this role of LPMOs, we further show that this effect can be extended to other ostensibly 'non-catalytic' proteins beyond LPMOs, such as bovine serum albumin and lactate dehydrogenase.

CHEMSUSCHEM, 2024. DOI: 10.1002/cssc.202401350 Early Access Date: NOV 2024

[P275-2024] "Properties of charge recombination in liquid argon"

Segreto, E.*

Liquid argon is an excellent medium for detecting particles, given its yields and transport properties of light and charge. The technology of liquid argon time projection chambers has reached its full maturity after four decades of continuous developments and is, or will be, used in world class experiments for neutrino and dark matter searches. The collection of ionization charge in these detectors allows to perform a complete tridimensional reconstruction of the tracks of charged particles, calorimetric measurements, particle identification. This work proposes an innovative approach to the problem of charge recombination in liquid argon which moves from a microscopic model and is applied to the cases of low energy electrons, alpha particles, and nuclear recoils. It takes inspiration and expands the recombination models commonly used by the liquid argon community. The model is able to describe precisely several sets of experimental data available in the literature, over wide ranges of electric field strengths and kinetic energies and can be easily extended to other particles.

PHYSICAL REVIEW D 110[6], 062002, 2024. DOI: 10.1103/PhysRevD.110.062002

[P276-2024] "Quantum mechanical analysis of newly synthesized HIV-1 protease inhibitors: evaluation of wild-type and resistant strain binding interactions"

Silva, G. V. R.; Reiniger, K. A. R.; Menezes, G. de L.; **Bezerra, K. S.*; Galvao, D. S.***; Saivish, M. V.; Silva, R. A. da; Akash, S.; Tayyeb, J. Z.; Oliveira, J. I. N.; Fulco, U. L.

Inhibition of HIV-1 protease is a cornerstone of antiretroviral therapy. However, the notorious ability of HIV-1 to develop resistance to protease inhibitors (PIs), particularly darunavir (DRV), poses a major challenge. Using quantum chemistry and computer simulations, this study aims to investigate the interactions between two novel PIs, GRL-004 and GRL-063, as well as a wild-type (WT) HIV strain and a DRV-resistant mutant strain. To do this, we used molecular docking, molecular dynamics simulations, and quantum mechanical calculations to check how well GRL-004 and GRL-063 bound to both WT and DRV-resistant proteases. The results show that GRL-004 and GRL-063 bind very well to ASP29 in the WT strain. ASP29 is an important amino acid in the HIV protease dimer. Remarkably, amino acids such as ILE50 in the WT strains showed substantial binding energies to both drugs. Quantum energy calculations showed a slight reduction in the energy affinity of the interaction between the MUT strain and the ligand GRL-063, compared to the WT strain. GRL-004 showed similar interaction energy for both strains, suggesting that it has greater plasticity than GRL-063 despite its lower interaction affinity. Furthermore, GLY49B demonstrated strong binding energies regardless of mutations. Other relevant residues with strong binding energies include GLY49B, PHE82A, PRO81A, ASP29A, ASP25A and ALA28B. This study improves our understanding of receptor-ligand dynamics and the adaptability of new protease inhibitors (PIs), which has profound implications for the innovation of future antiretroviral drugs. Inhibition of HIV-1 protease is a cornerstone of antiretroviral therapy.

PHYSICAL CHEMISTRY CHEMICAL PHYSICS 26[42], 26748-26764, 2024. DOI: 10.1039/d4cp02895c

[P277-2024] "Scintillation light in SBND: simulation, reconstruction, and expected performance of the photon detection system"

Abratenko, P.; Acciarri, R.; Adams, C.; **Machado, A.*; Pimentel, V. L.*; Segreto, E.***; et al.
SBND Collaboration

SBND is the near detector of the Short-Baseline Neutrino program at Fermilab. Its location near to the Booster Neutrino Beam source and relatively large mass will allow the study of neutrino interactions on argon with unprecedented statistics. This paper describes the expected performance of the SBND photon detection system, using a simulated sample of beam neutrinos and cosmogenic particles. Its design is a dual readout concept combining a system of 120 photomultiplier tubes, used for triggering, with a system of 192 X-ARAPUCA devices, located behind the anode wire planes. Furthermore, covering the cathode plane with highly-reflective panels coated with a wavelength-shifting compound recovers part of the light emitted towards the cathode, where no optical detectors exist. We show how this new design provides a high light yield and a more uniform detection efficiency, an excellent timing resolution and an independent 3D-position reconstruction using only the scintillation light. Finally, the whole reconstruction chain is applied to recover the temporal structure of the beam spill, which is resolved with a resolution on the order of nanoseconds.

EUROPEAN PHYSICAL JOURNAL C 84[10], 1046, 2024. DOI: 10.1140/epjc/s10052-024-13306-3

[P278-2024] "Search for a new resonance decaying into two spin-0 bosons in a final state with two photons and two bottom quarks in proton-proton collisions at √s=13 TeV"

Tumasyan, A.; Adam, W.; Andrejkovic, J. W.; **Chinellato, J. A.***; et al.
CMS Collaboration

A search for a new boson X is presented using CERN LHC proton-proton collision data collected by the CMS experiment at root s = 13 TeV in 2016-2018, and corresponding to an integrated luminosity of 138 fb(-1). The resonance X decays into either a pair of Higgs bosons HH of mass 125 GeV or an H and a new spin-0 boson Y. One H subsequently decays to a pair of photons, and the second H or Y, to a pair of bottom quarks. The explored mass ranges of X are 260-1000 GeV and 300-1000 GeV, for decays to HH and to HY, respectively, with the Y mass range being 90-800 GeV. For a spin-0 X hypothesis, the 95% confidence level upper limit on the product of its production cross section and decay branching fraction is observed to be within 0.90-0.04 fb, depending on the masses of X and Y. The largest deviation from the background-only hypothesis with a local (global) significance of 3.8 (below 2.8) standard deviations is observed for X and Y masses of 650 and 90 GeV, respectively. The limits are interpreted using several models of new physics.

JOURNAL OF HIGH ENERGY PHYSICS [5], 316, 2024. DOI: 10.1007/JHEP05(2024)316

[P279-2024] "Search for a third-generation leptoquark coupled to a τ lepton and a b quark through single, pair, and nonresonant production in proton-proton collisions at √s=13 TeV"

Hayrapetyan, A.; Tumasyan, A.; Adam, W.; **Chinellato, J. A.*;** et al.
CMS Collaboration

A search is presented for a third-generation leptoquark (LQ) coupled exclusively to a tau lepton and a b quark. The search is based on proton-proton collision data at a center-of-mass energy of 13 TeV recorded with the CMS detector, corresponding to an integrated luminosity of 138 fb(-1). Events with tau leptons and a varying number of jets originating from b quarks are considered, targeting the single and pair production of LQs, as well as nonresonant t-channel LQ exchange. An excess is observed in the data with respect to the background expectation in the combined analysis of all search regions.

For a benchmark LQ mass of 2 TeV and an LQ-b-tau coupling strength of 2.5, the excess reaches a local significance of up to 2.8 standard deviations. Upper limits at the 95% confidence level are placed on the LQ production cross section in the LQ mass range 0.5-2.3 TeV, and up to 3 TeV for t-channel LQ exchange. Leptoquarks are excluded below masses of 1.22-1.88 TeV for different LQ models and varying coupling strengths up to 2.5. The study of nonresonant tau tau production through t-channel LQ exchange allows lower limits on the LQ mass of up to 2.3 TeV to be obtained.<fig id="Figa" position="anchor"

JOURNAL OF HIGH ENERGY PHYSICS [5], 311, 2024. DOI: 10.1007/JHEP05(2024)311

[P280-2024] "Search for Baryon Number Violation in Top Quark Production and Decay Using Proton-Proton Collisions at √ s=13 TeV"

Hayrapetyan, A.; Tumasyan, A.; Adam, W.; **Chinellato, J. A.***; et al.
CMS Collaboration

A search is presented for baryon number violating interactions in top quark production and decay. The analysis uses data from proton-proton collisions at a center-of-mass energy of 13 TeV, collected with the CMS detector at the LHC with an integrated luminosity of 138 fb-1. Candidate events are selected by requiring two oppositely charged leptons (electrons or muons) and exactly one jet identified as originating from a bottom quark. Multivariate discriminants are used to separate the signal from the background. No significant deviation from the standard model prediction is observed. Upper limits are placed on the strength of baryon number violating couplings. For the first time the production of single top quarks via baryon number violating interactions is studied. This allows the search to set the most stringent constraints to date on the branching fraction of the top quark decay to a lepton, an up-type quark (u or c), and a downtype quark (d, s, or b). The results improve the previous bounds by 3 to 6 orders of magnitude based on the fermion flavor combination of the baryon number violating interactions.

PHYSICAL REVIEW LETTERS 132[24], 2024. DOI: 10.1103/PhysRevLett.132.241802

[P281-2024] "Search for exotic decays of the Higgs boson to a pair of pseudoscalars in the μμbb and ττbb final states"

Hayrapetyan, A.; Tumasyan, A.; Adam, W.; **Chinellato, J. A.***; et al.
CMS Collaboration

A search for exotic decays of the Higgs boson (H) with a mass of 125 GeV to a pair of light pseudoscalars a(1) is performed in final states where one pseudoscalar decays to two b quarks and the other to a pair of muons or tau leptons. A data sample of proton-proton collisions at root s = 13 TeV corresponding to an integrated luminosity of 138 fb(-1) recorded with the CMS detector is analyzed. No statistically significant excess is observed over the standard model backgrounds. Upper limits are set at 95% confidence level (CL) on the Higgs boson branching fraction to mu mu bb and to tau tau bb, via a pair of a(1)s. The limits depend on the pseudoscalar mass m(a1) and are observed to be in the range (0.17-3.3) x10(-4) and (1.7-7.7) x10(-2) in the mu mu bb and tau tau bb final states, respectively. In the framework of models with two Higgs doublets and a complex scalar singlet (2HDM+S), the results of the two final states are combined to determine upper limits on the branching fraction B(H -> a(1)a(1) -> llbb) at 95% CL, with l being a muon or a tau lepton. For different types of 2HDM+S, upper bounds on the branching fraction B(H -> a(1) a(1)) are extracted from the combination of the two channels. In most of the Type II 2HDM+S parameter space, B(H -> a(1) a(1)) values above 0.23 are excluded at 95% CL for m(a1) values between 15 and 60 GeV.

EUROPEAN PHYSICAL JOURNAL C 84[5], 493, 2024. DOI: 10.1140/epjc/s10052-024-12727-4

[P282-2024] "Search for heavy neutral leptons in final states with electrons, muons, and hadronically decaying tau leptons in proton-proton collisions at √s=13 TeV"

Hayrapetyan, A.; Tumasyan, A.; Adam, W.; **Chinellato, J. A.***; et al.
CMS Collaboration

A search for heavy neutral leptons (HNLs) of Majorana or Dirac type using proton-proton collision data at root s = 13TeV= 13 TeV is presented. The data were collected by the CMS experiment at the CERN LHC and correspond to an integrated luminosity of 138 fb(-1). Events with three charged leptons (electrons, muons, and hadronically decaying tau leptons) are selected, corresponding to HNL production in association with a charged lepton and decay of the HNL to two charged leptons and a standard model (SM) neutrino. The search is performed for HNL masses between 10 GeV and 1.5 TeV. No evidence for an HNL signal is observed in data. Upper limits at 95% confidence level are found for the squared coupling strength of the HNL to SM neutrinos, considering exclusive coupling of the HNL to a single SM neutrino generation, for both Majorana and Dirac HNLs. The limits exceed previously achieved experimental constraints for a wide range of HNL masses, and the limits on tau neutrino coupling scenarios with HNL masses above the W boson mass are presented for the first time.

JOURNAL OF HIGH ENERGY PHYSICS [6], 123, 2024. DOI: 10.1007/JHEP06(2024)123

[P283-2024] "Search for jet quenching effects in high-multiplicity pp collisions at √s=13 TeV via di-jet acoplanarity"

Acharya, S.; Adamova, D.; Rinella, G. A.; **Chinellato, D. D.*; Guardiano, G. G.*; Liveraro, G. S. S.*; Takahashi, J.***; et al.
ALICE Collaboration

The ALICE Collaboration reports a search for jet quenching effects in highmultiplicity (HM) proton-proton collisions at root s = 13TeV, using the semi-inclusive azimuthaldifference distribution Delta phi of charged-particle jets recoiling from a high transverse momentum (high- pT,trig) trigger hadron. Jet quenching may broaden the Delta phi distribution measured in HM events compared to that in minimum bias (MB) events. The measurement employs a pT,trig-differential observable for data-driven suppression of the contribution of multiple partonic interactions, which is the dominant background. While azimuthal broadening is indeed observed in HM compared to MB events, similar broadening for HM events is observed for simulations based on the PYTHIA 8 Monte Carlo generator, which does not incorporate jet quenching. Detailed analysis of these data and simulations show that the azimuthal broadening is due to bias of the HM selection towards events with multiple jets in the final state. The identification of this bias has implications for all jet quenching searches where selection is made on the event activity.

JOURNAL OF HIGH ENERGY PHYSICS [5], 229, 2024. DOI: 10.1007/JHEP05(2024)229

[P284-2024] "Search for long-lived heavy neutral leptons decaying in the CMS muon detectors in proton-proton collisions at √s=13 TeV"

Hayrapetyan, A.; Tumasyan, A.; Adam, W.; **Chinellato, J. A.***; et al.
CMS Collaboration

A search for heavy neutral leptons (HNLs) decaying in the CMS muon system is presented. A data sample is used corresponding to an integrated luminosity of 138 fb(-1) of proton-proton collisions at root s = 13 TeV, recorded at the CERN LHC in 2016-2018. Decay products of long-lived HNLs could interact with the shielding materials in the CMS muon system and create hadronic and electromagnetic showers detected in the muon chambers. This distinctive signature provides a unique handle to search for HNLs with masses below 4 GeV and proper decay lengths of the order of meters. The signature is sensitive to HNL couplings to all three generations of leptons. Candidate events are required to contain a prompt electron or muon originating from a vertex on the beam axis and a displaced shower in the muon chambers. No significant deviations from the standard model background expectation are observed. In the electron (muon) channel, the most stringent limits to date are set for HNLs in the mass range of 2.1-3.0 (1.9-3.3) GeV, reaching mixing matrix element squared values as low as 8.6(4.6) x 10(-6).

PHYSICAL REVIEW C 110[1], 012004, 2024. DOI: 10.1103/PhysRevD.110.012004

[P285-2024] "Search for long-lived heavy neutrinos in the decays of B mesons produced in proton-proton collisions at √s=13 TeV"

Hayrapetyan, A.; Tumasyan, A.; Adam, W.; **Chinellato, J. A.***; et al.
CMS Collaboration

A search for long-lived heavy neutrinos (N) in the decays of B mesons produced in proton-proton collisions at root s = 13 TeV is presented. The data sample corresponds to an integrated luminosity of 41.6 fb(-1) collected in 2018 by the CMS experiment at the CERN LHC, using a dedicated data stream that enhances the number of recorded events containing B mesons. The search probes heavy neutrinos with masses in the range 1 < m(N) < 3 GeV and decay lengths in the range 10(-2) < c tau(N) < 10(4) mm, where tau(N) is the N proper mean lifetime. Signal events are defined by the signature B -> l(B)NX; N -> l(+/-)pi(-/+), where the leptons l(B) and l can be either a muon or an electron, provided that at least one of them is a muon. The hadronic recoil system, X, is treated inclusively and is not reconstructed. No significant excess of events over the standard model background is observed in any of the l(+/-)pi(-/+) invariant mass distributions. Limits at 95% confidence level on the sum of the squares of the mixing amplitudes between heavy and light neutrinos, vertical bar V-N vertical bar(2), and on c tau(N) are obtained in different mixing scenarios for both Majorana and Dirac-like N particles. The most stringent upper limit vertical bar V-N vertical bar(2) < 2.0 x 10(-5) is obtained at m(N) = 1.95 GeV for the Majorana case where N mixes exclusively with muon neutrinos. The limits on vertical bar V-N vertical bar(2) for masses 1 < m(N) < 1.7 GeV are the most stringent from a collider experiment to date.

JOURNAL OF HIGH ENERGY PHYSICS [6], 183, 2024. DOI: 10.1007/JHEP06(2024)183

[P286-2024] "Search for long-lived particles decaying to final states with a pair of muons in proton-proton collisions at √s=13.6 TeV"

Hayrapetyan, A.; Tumasyan, A.; Adam, W.; **Chinellato, J. A.***; et al.
CMS Collaboration

An inclusive search for long-lived exotic particles (LLPs) decaying to final states with a pair of muons is presented. The search uses data corresponding to an integrated luminosity of 36.6 fb(-1) collected by the CMS experiment from the proton-proton collisions at root s - 13.6TeV in 2022, the first year of Run 3 of the CERN LHC. The experimental signature is a pair of oppositely charged muons originating from a secondary vertex spatially separated from the proton-proton interaction point by distances ranging from several hundred mu m to several meters. The sensitivity of the search benefits from new triggers for displaced dimuons developed for Run 3. The results are interpreted in the framework of the hidden Abelian Higgs model, in which the Higgs boson decays to a pair of long-lived dark photons, and of an R-parity violating supersymmetry model, in which long-lived neutralinos decay to a pair of muons and a neutrino. The limits set on these models are the most stringent to date in wide regions of lifetimes for LLPs with masses larger than 10 GeV.

JOURNAL OF HIGH ENERGY PHYSICS [5], 047, 2024. DOI: 10.1007/JHEP05(2024)047

[P287-2024] "Search for Narrow Trijet Resonances in Proton-Proton Collisions at √s=13 TeV"

Hayrapetyan, A.; Tumasyan, A.; Adam, W.; **Chinellato, J. A.***; et al.
CMS Collaboration

The first search for singly produced narrow resonances decaying to three well-separated hadronic jets is presented. The search uses proton-proton collision data corresponding to an integrated luminosity of 138 fb(-1) at root s = 13 TeV, collected at the CERN LHC. No significant deviations from the background predictions are observed between 1.75 and 9.00 TeV. The results provide the first mass limits on a right-handed boson Z(R) decaying to three gluons and on an excited quark decaying via a vector boson to three quarks, as well as updated limits on a Kaluza-Klein gluon decaying via a radion to three gluons.

PHYSICAL REVIEW LETTERS 133[1], 011801, 2024. DOI: 10.1103/PhysRevLett.133.011801

[P288-2024] "Search for stealth supersymmetry in final st.ates with two photons, jets, and low missing transverse momentum in proton-proton collisions at √s=13 TeV"

Hayrapetyan, A.; Tumasyan, A.; Adam, W.; **Chinellato, J. A.***; et al.
CMS Collaboration

The results of a search for stealth supersymmetry in final states with two photons and jets, targeting a phase space region with low missing transverse momentum (p(miss) (T)), are reported. The study is based on a sample of proton-proton collisions at root s = 13 TeV collected by the CMS experiment, corresponding to an integrated luminosity of 138 fb(-1). As LHC results continue to constrain the parameter space of the minimal supersymmetric standard model, the low pmiss T regime is increasingly valuable to explore. To estimate the backgrounds due to standard model processes in such events, we apply corrections derived from simulation to an estimate based on a control selection in data. The results are interpreted in the context of simplified stealth supersymmetry models with gluino and squark pair production. The observed data are consistent with the standard model predictions, and gluino (squark) masses of up to 2150 (1850) GeVare excluded at the 95% confidence level.

PHYSICAL REVIEW D 109[11], 112009, 2024. DOI: 10.1103/PhysRevD.109.112009

[P289-2024] "Search for the Chiral Magnetic Effect with charge-dependent azimuthal correlations in Xe-Xe collisions at √SNN=5.44 TeV"

Acharya, S.; Adamova, D.; Adler, A.; **Chinellato, D. D.*; Guardiano, G. G.*; Jahnke, C.*; Takahashi, J.***; et al.
ALICE Collaboration

Charge-dependent two- and three-particle correlations measured in Xe-Xe collisions at root S-NN = 5.44 TeV are presented. Results are obtained for charged particles in the pseudorapidity range |eta| < 0.8 and transverse momentum interval 0.2 <= p(T) < 5.0 GeV/c for different collision centralities. The three-particle correlator gamma(alpha beta)=< cos(phi(alpha) +phi(beta) - 2 psi(2))>, calculated for different combinations of charge sign alpha and beta, is expected to be sensitive to the presence of the Chiral Magnetic Effect (CME). Its magnitude is similar to the one observed in Pb-Pb collisions in contrast to a smaller CME signal in Xe-Xe collisions than in Pb-Pb collisions predicted by Monte Carlo (MC) calculations including a magnetic field induced by the spectator protons. These observations point to a large nonCME contribution to the correlator. Furthermore, the charge dependence of gamma(alpha beta) can be described by a blast wave model calculation that incorporates background effects and by the Anomalous Viscous Fluid Dynamics model with values of the CME signal consistent with zero. The Xe-Xe and Pb-Pb results are combined with the expected CME signal dependence on the system size from the MC calculations including a magnetic field to obtain the fraction of CME contribution in gamma(alpha beta), f(CME). The CME fraction is compatible with zero for the 30% most central events in both systems and then becomes positive. This yields an upper limit of 2% (3%) and 25% (32%) at 95% (99.7%) confidence level for the CME signal contribution to gamma(alpha beta) in the 0-70% Xe-Xe and Pb-Pb collisions, respectively.

PHYSICS LETTERS B 856, 138862, 2024. DOI: 10.1016/j.physletb.2024.138862

[P290-2024] "Search for the lepton flavor violating τ -- 3μ decay in proton-proton collisions at √s=13 TeV"

Hayrapetyan, A.; Tumasyan, A.; Adam, W.; **Chinellato, J. A.***; et al.
CMS Collaboration

A search for the lepton flavor violating tau -> 3 mu decay is performed using proton-proton collision events at a center-of--mass energy of 13 TeV collected by the CMS experiment at the LHC in 2017-2018, corresponding to an integrated luminosity of 97.7 fb(-1). Tau leptons produced in both heavy-flavor hadron and W boson decays are exploited in the analysis. No evidence for the decay is observed. The results of this search are combined with an earlier null result based on data collected in 2016 to obtain a total integrated luminosity of 131 fb(-1). The observed (expected) upper limits on the branching fraction.(tau -> 3 mu) at confidence levels of 90 and 95% are 2.9 x 10(-8) (2.4 x 10(-8)) and 3.6 x 10(-8) (3.0 x 10(-8)), respectively.

PHYSICS LETTERS B 853, 138633, 2024. DOI: 10.1016/j.physletb.2024.138633

[P291-2024] "Selective Hydrogenation Promotes the Anisotropic Thermoelectric Properties of TPDH-Graphene"

Oliveira, C. C.; **Galvao, D. S.***; Autreto, P. A. S.

We have combined density functional theory calculations with the Boltzmann semiclassical transport theory to investigate the effect of selective hydrogenation on the thermoelectric properties of tetra-penta-decahexagonal graphene (TPDH-gr), a recently proposed new two-dimensional carbon allotrope. Our results show that the Seebeck coefficient is enhanced after hydrogenation. The conductivity along the x direction is increased almost eight times while being almost suppressed along the y direction. This behavior can be understood in terms of the electronic structure changes due to the appearance of a Dirac-like cone after selective hydrogenation. Consistent with the literature, the electronic contribution to the thermal conductivity displays the same qualitative behavior as the conductivity, as expected from the Wiedemann-Franz law. The increase in thermal conductivity with temperature limits the material's power factor. The significant increases in the Seebeck coefficient and conductivity also contribute to the thermal conductivity increase. These results show that hydrogenation is an effective method to improve the TPDH--gr thermoelectric properties, and this carbon allotrope can be an effective material for thermoelectric applications.

JOURNAL OF PHYSICAL CHEMISTRY C 128[15], 6206-6212, 2024. DOI: 10.1021/acs.jpcc.4c00175

[P292-2024] "Structural and electronic properties of amorphous silicon and germanium monolayers and nanotubes: A DFT investigation"

Tromer, R. M.; Pereira Jr., M. L.; Ribeiro Jr., L. A.; **Galvao, D. S.***

A recent breakthrough has been achieved by synthesizing monolayer amorphous carbon (MAC). Here, we used ab initio (DFT) molecular dynamics simulations to study silicon and germanium MAC analogs. Typical unit cells contain more than 600 atoms. We also considered their corresponding nanotube structures. The cohesion energy values for MASi and MAGe are approximately 3.0 eV/atom lower than the energy ordering of silicene and germanene, respectively. Their electronic behavior varies from metallic to small band gap semiconductors. Since silicene, germanene, and MAC have already been experimentally realized, the corresponding MAC-like versions we propose are within our present synthetic capabilities.

CHEMICAL PHYSICS LETTERS 856, 141647, 2024. DOI: 10.1016/j.cplett.2024.141647 Early Access Date: SEP 2024

[P293-2024] "Test of lepton flavor universality in B± -- K± μ+μ- and B± -- K± e+ e- decays in proton-proton collisions at √s=13 TeV"

Hayrapetyan, A.; Tumasyan, A.; Adam, W.; **Chinellato, J. A.***; et al.
CMS Collaboration

A test of lepton flavor universality in B-+/- -> K +/- mu(+) mu(-) and B-+/- -> (K)+/- e(+) e(-) decays, as well as a measurement of differential and integrated branching fractions of a nonresonant B-+/- -> K-+/- mu(+)mu(-) decay are presented. The analysis is made possible by a dedicated data set of proton--proton collisions at root s = 13 TeV recorded in 2018, by the CMS experiment at the LHC, using a special high-rate data stream designed for collecting about 10 billion unbiased b hadron decays. The ratio of the branching fractions B(B-+/- -> K-+/- mu(+) mu(-)) to B(B-+/- -> K-+/- e(+) e(-)) is determined from the measured double ratio R(K) of these decays to the respective branching fractions of the B-+/- -> J/psi K-+/- with J/psi -> mu(+)mu(-) and e(+) e(-) decays, which allow for significant cancellation of systematic uncertainties. The ratio R(K) is measured in the range 1.1 < q(2) < 6.0 GeV2, where q is the invariant mass of the lepton pair, and is found to be R(K) = 0.78(-0.23)(+0.47), in agreement with the standard model expectation R(K) approximate to 1. This measurement is limited by the statistical precision of the electron channel. The integrated branching fraction in the same q(2) range, B(B-+/- -> K-+/- mu(+) mu(-)) = (12.42 +/- 0.68) x 10(-8), is consistent with the present world-average value and has a comparable precision.

REPORTS ON PROGRESS IN PHYSICS 87[7], 077802, 2024. DOI: 10.1088/1361-6633/ad4e65

[P294-2024] "The ALICE experiment: a journey through QCD"

Acharya, S.; Adamová, D.; Adler, A.; **Chinellato, D. D.*; Guardiano, G. G.*; Jahnke, C.*; Takahashi, J.***; et al.
ALICE Collaboration

The ALICE experiment was proposed in 1993, to study strongly-interacting matter at extreme energy densities and temperatures. This proposal entailed a comprehensive investigation of nuclear collisions at the LHC. Its physics programme initially focused on the determination of the properties of the quark-gluon plasma (QGP), a deconfined state of quarks and gluons, created in such collisions. The ALICE physics programme has been extended to cover a broader ensemble of observables related to Quantum Chromodynamics (QCD), the theory of strong interactions. The experiment has studied Pb--Pb, Xe-Xe, p-Pb and pp collisions in the multi-TeV centre of mass energy range, during the Run 1-2 data-taking periods at the LHC (2009-2018). The aim of this review is to summarise the key ALICE physics results in this endeavor, and to discuss their implications on the current understanding of the macroscopic and microscopic properties of strongly-interacting matter at the highest temperatures reached in the laboratory. It will review the latest findings on the properties of the QGP created by heavy-ion collisions at LHC energies, and describe the surprising QGP-like effects in pp and p-Pb collisions. Measurements of few-body QCD interactions, and their impact in unraveling the structure of hadrons and hadronic interactions, will be discussed. ALICE results relevant for physics topics outside the realm of QCD will also be touched upon. Finally, prospects for future measurements with the ALICE detector in the context of its planned upgrades will also be briefly described.

EUROPEAN PHYSICAL JOURNAL C 84[8], 813, 2024. DOI: 10.1140/epjc/s10052-024-12935-y

[P295-2024] "The SRG/eROSITA All-Sky Survey Dark Energy Survey year 3 weak gravitational lensing by eRASS1 selected galaxy clusters"

Grandis, S.; Ghirardini, V.; Bocquet, S.; **Navarro-Alsina, A.***; et al.
Dark Energy Survey Collaboration

Context. Number counts of galaxy clusters across redshift are a powerful cosmological probe if a precise and accurate reconstruction of the underlying mass distribution is performed - a challenge called mass calibration. With the advent of wide and deep photometric surveys, weak gravitational lensing (WL) by clusters has become the method of choice for this measurement. Aims. We measured and validated the WL signature in the shape of galaxies observed in the first three years of the Dark Energy Survey (DES Y3) caused by galaxy clusters and groups selected in the first all-sky survey performed by SRG (Spectrum Roentgen Gamma)/eROSITA (eRASS1). These data were then used to determine the scaling between the X-ray photon count rate of the clusters and their halo mass and redshift. Methods. We empirically determined the degree of cluster member contamination in our background source sample. The individual cluster shear profiles were then analyzed with a Bayesian population model that self-consistently accounts for the lens sample selection and contamination and includes marginalization over a host of instrumental and astrophysical systematics. To quantify the accuracy of the mass extraction of that model, we performed mass measurements on mock cluster catalogs with realistic synthetic shear profiles. This allowed us to establish that hydrodynamical modeling uncertainties at low lens redshifts ($z < 0.6$) are the dominant systematic limitation. At high lens redshift, the uncertainties of the sources' photometric redshift calibration dominate. Results. With regard to the X-ray count rate to halo mass relation, we determined its amplitude, its mass trend, the redshift evolution of the mass trend, the deviation from self-similar redshift evolution, and the intrinsic scatter around this relation. Conclusions. The mass calibration analysis performed here sets the stage for a joint analysis with the number counts of eRASS1 clusters to constrain a host of cosmological parameters. We demonstrate that WL mass calibration of galaxy clusters can be performed successfully with source galaxies whose calibration was performed primarily for cosmic shear experiments, opening the way for the cluster cosmological exploitation of future optical and NIR surveys like Euclid and LSST.

ASTRONOMY & ASTROPHYSICS 687, A178, 2024. DOI: 10.1051/0004-6361/202348615

[P296-2024] "Track signals at IceCube from subleading channels"

Francener, R.; Gonsalves, V. P.; **Gratieri, D. R.***

Tracks events at the IceCube Observatory are characterized by an energetic muon crossing several kilometers before decaying. Such muons are dominantly produced in charged current (CC) muon neutrinohadron interactions. However, muons are also produced through W-boson production and in the decay of tau leptons and heavy mesons created in neutral and charged current interactions induced by all neutrino flavors. In this paper, we investigate the contribution of these subleading channels to events characterized as tracks at the IceCube. Our results indicate that these channels correspond to a non-negligible fraction of the high-energy starting events track events. In addition, we show that its contributions are concentrated in muons that are less energetic than those arising from muonic neutrino CC interactions for the same visible energies of the process. Finally, we investigate the impact of these additional channels on the description of the astrophysical neutrino flux, and we find that the inclusion of these subleading processes are important in determining the parameters of the astrophysical neutrino flux.

PHYSICAL REVIEW D 110[5], 053011, 2024. DOI: 10.1103/PhysRevD.110.053011

[P297-2024] "Tracking of charged particles with nanosecond lifetimes at LHCb"

Aaij, R.; Abdelmotteleb, A. S. W.; Beteta, C. A.; **Magalhaes, P. C.***; et al.
LHCb Collaboration

A method is presented to reconstruct charged particles with lifetimes between 10 ps and 10 ns, which considers a combination of their decay products and the partial tracks created by the initial charged particle. Using the Xi(-) baryon as a benchmark, the method is demonstrated with simulated events and proton-proton collision data at root s = 13 TeV, corresponding to an integrated luminosity of 2.0 fb(-1) collected with the LHCb detector in 2018. Significant improvements in the angular resolution and the signal purity are obtained. The method is implemented as part of the LHCb Run 3 event trigger in a set of requirements to select detached hyperons. This is the first demonstration of the applicability of this approach at the LHC, and the first to show its scaling with instantaneous luminosity.

EUROPEAN PHYSICAL JOURNAL C 84[7], 761, 2024. DOI: 10.1140/epjc/s10052-024-12993-2

[P298-2024] "Tunable Degenerate Optical Parametric Oscillation with Coupled Microresonators"

Tomazio, N. B.*; Trinchao, L. O.*; Gonçalves, E. S.*; Santos, L. F. dos*; Santos, F. G. S.*; Jarschel, P. F.*; Alegre, T. P. M.*; Wiederhecker, G. S.*

Microresonator-based degenerate optical parametric oscillation (DOPO) has recently been explored as a compelling platform for all-optical computing and quantum information applications such as truly random number generation and the production of squeezed states of light. Emerging research has highlighted the potential of coupled microresonators, or photonic molecules, as a novel avenue for spectral engineering, unlocking an extra degree of freedom for the optimization of four-wave mixing interactions. Here, we demonstrate a single tunable DOPO within the coupled modes of a silicon nitride triplet-state photonic molecule. Our design introduces a distinctive mechanism for spectral engineering, using microheaters to individually tune the resonance spectral positions, thus enabling dynamic local dispersion control within the coupled modes. We successfully generated a DOPO signal with active efficiency control and explored the optical mode spacing in the tens of gigahertz range to use native phase--locked optical pumps driven by a radio frequency source.

ACS PHOTONICS, 2024. DOI: 10.1021/acsphotonics.4c01559 Early Access Date: NOV 2024

[P299-2024] "Tuning the antiferromagnetic ground state of Ce2RhIn8 by Ga substitution"

Caffer, A. M.*; Ajeesh, M. O.; **Carvalho, M. H.*; Mercena, S. G.*; Freitas, G. S*.; Pizzi, H. B.*; Passos, D. S.*; Adriano, C.***; Bauer, E. D.; Thompson, J. D.; Ronning, F.; Thomas, S. M.; Rosa, P. F. S.; **Pagliuso, P. G.***

We explore the effect of Ga substitution on the physical properties of single crystals of Ce2RhIn8 through measurements of temperature-dependent specific heat, magnetic susceptibility, and electrical resistivity. Our data on Ce2RhIn8-xGax, single crystals reveal a monotonic decrease of the antiferromagnetic transition temperature from TN = 2.77 K for the parent compound to TN = 1.96 K for the highest Ga concentration achieved (x = 0.55). To understand the evolution of the crystalline electric field (CEF) scheme and exchange interactions as a function of Ga substitution, we fit our thermodynamic data to a Hamiltonian containing a tetragonal CEF term and meanfield isotropic exchange terms. Our results show a systematic increase in the energies of the first and second excited states as a function of Ga concentration. Moreover, we find significant changes to the CEF ground-state (GS) wave function (P = alpha | +/- 5/2) + /1 - alpha 2 | +3/2)), including an increase in the alpha coefficient and in the | B02 | CEF parameter, with increasing Ga concentration. This evolution of the GS wave function drives the system away from the quantum critical point, whereas the chemical pressure associated with the Ga substitution drives the system towards it. Such behavior raises the question of whether pressure-induced superconductivity can be stabilized in this system. Our electrical resistivity and heat capacity measurements on Ce2RhIn7.64Ga0.36 under hydrostatic pressure reveal a zero-resistance state; however, no bulk superconductivity is detected. These results suggest that the occurrence of bulk superconductivity may be unfavorable in this system due to the observed CEF GS wave-function evolution and/or to the pair-breaking mechanism in the Ce2RhIn8-xGax series.

PHYSICAL REVIEW B 110[20], 205105, 2024. DOI: 10.1103/PhysRevB.110.205105

[P300-2024] "Tuning the band gap of manganese telluride quantum dots (MnTe QDs) for photocatalysis"

Gowda, C. C.; Chandravanshi, D.; **Tromer, R. M.***; Malya, A.; Chattopadhyay, K.; **Galvao, D. S.***; Tiwary, C. S.

Laser ablation synthesis in solution (LASiS) was used to synthesize quantum dots (QDs) of manganese telluride (MnTe). Size--tuneable QDs exhibit physicochemical property variation in the bandgap, optical, electrical, and magnetic properties. The size of QDs was fine-tuned with varying power and time duration of laser ablation. The characteristics of MnTe QDs were investigated using basic structural and morphological characterizations. The observed bandgap opening in the material is due to the quantum confinement effect, which led to increased energy band separation, as predicted from DFT simulations. The magnetic property of the synthesized MnTe QD catalysts influences the degradation process, with the process following pseudo--first-order kinetics. The photocatalytic dye degradation was studied using UV-visible spectroscopy. MnTe QDs were able to photodegrade methylene blue reagent up to 93.4% in 60 min under an external magnetic field. The magnetic field-induced MnTe QDs showed enhanced photocatalytic degradation efficiency with increased apparent rate kinetics up to ten times (0.0453 min-1) compared to just sunlight exposure (0.00456 min-1).Graphical Abstract(a) HAADF-STEM of the synthesized MnTe QD dispersed, (b) SEM image of the same, (c) relative concentration of the samples with and without magnetic fields, inset: photo degraded samples on exposure of magnetic fields and (d) schematic representation of the photocatalytic dye-degradation.

APPLIED PHYSICS A-MATERIALS SCIENCE & PROCESSING 130[5], 299, 2024. DOI: 10.1007/s00339-024-07378-x

[P301-2024] "Visible Light-Driven Photocatalysis and Antibacterial Performance of a Cu-TiO2 Nanocomposite"

Lima, M. S. de; Schio, A. L.; Aguzzoli, C.; Souza, W. V. de; Roesch-Ely, M.; **Leidens, L. M.*; Boeira, C. D.*; Alvarez, F.***; Elois, M. A.; Fongaro, G.; Figueroa, C. A.; Michels, A. F.

A Cu-TiO2 nanomaterial with unique antibacterial and photocatalytic properties is introduced in this study. Cu-TiO2 nanocomposites were obtained using an adapted direct current magnetron sputtering apparatus, where TiO2 anatase nanoparticles (NPs) were used as the substrates and copper as the sputtering target. The obtained powder was characterized by physical and chemical methods. Copper was deposited on TiO2 NPs for 30 and 60 min, resulting in two samples with different copper contents of 3 and 5 wt %, respectively. The photocatalysis test evaluated the degradation of rhodamine B (RhB) dye under a specific wavelength (405 nm LED) and a complete degeneration occurred in 120 min, similar to 33% faster when compared to pristine TiO2. The antibacterial assays were performed for Escherichia coli and Staphylococcus aureus in dark and visible--light conditions, using a 405 nm LED and a wide-spectrum white LED, reaching an inactivation of 99.9999% for both bacteria. The magnetron sputtering is an ecofriendly way to form heterojunctions with photocatalytic and bactericidal properties in the absence of wet chemical methods or residues. This work may open new pathways for enhancing the fungicidal and virucidal activities of nanocomposites under the action of visible light.

ACS OMEGA 9[47], 47122-47134, 2024. DOI: 10.1021/acsomega.4c07515

[P302-2024] "Vortex rings in event-by-event relativistic heavy-ion collisions"

Chinellato, D. D.*; Lisa, M. A.; **Serenone, W. M.***; Shen, C.; **Takahashi, J.*; Torrieri, G.***

We present event-by-event simulations for central asymmetric light+heavy and Au+Au collisions to investigate the formation and evolution of vortex-ring structures in the longitudinal flow velocity profile.

The production-plane polarization of Lambda hyperons, defined with respect to the Lambda momentum and the beam, can track the “vortex-ring” feature in the event, a characteristic vortical structure generated by longitudinal flow gradients. We make comprehensive model predictions for the rapidity-dependent vortex-ring observables for different collision system sizes at root s(NN) = 200 and 72 GeV. Our predictions at the latter energy can be explored in the future LHCb fixed-target experiment at the Large Hadron Collider.

PHYSICAL REVIEW C 110[5], 054908, 2024. DOI: 10.1103/PhysRevC.110.054908

[P303-2024] “Weak lensing combined with the kinetic Sunyaev-Zel’dovich effect: a study of baryonic feedback”

Bigwood, L.; Amon, A.; Schneider, A.; **Navarro-Alsina, A.***; et al.

Extracting precise cosmology from weak lensing surveys requires modelling the non-linear matter power spectrum, which is suppressed at small scales due to baryonic feedback processes. However, hydrodynamical galaxy formation simulations make widely varying predictions for the amplitude and extent of this effect. We use measurements of Dark Energy Survey Year 3 weak lensing (WL) and Atacama Cosmology Telescope DR5 kinematic Sunyaev-Zel’dovich (kSZ) to jointly constrain cosmological and astrophysical baryonic feedback parameters using a flexible analytical model, ‘baryonification’. First, using WL only, we compare the constraints using baryonification to a simulation-calibrated halo model, a simulation-based emulator model, and the approach of discarding WL measurements on small angular scales. We find that model flexibility can shift the value of and degrade the uncertainty. The kSZ provides additional constraints on the astrophysical parameters, with the joint WL + kSZ analysis constraining S-8 = 0.823(-0.020)(+0.019). We measure the suppression of the non-linear matter power spectrum using WL + kSZ and constrain a mean feedback scenario that is more extreme than the predictions from most hydrodynamical simulations. We constrain the baryon fractions and the gas mass fractions and find them to be generally lower than inferred from X-ray observations and simulation predictions. We conclude that the WL + kSZ measurements provide a new and complementary benchmark for building a coherent picture of the impact of gas around galaxies across observations.

MONTHLY NOTICES OF THE ROYAL ASTRONOMICAL SOCIETY 534[1], 655-682, 2024. DOI: 10.1093/mnras/stae2100

Eventos publicados

[P304-2024] “A solvable two-dimensional swarmalator model”

O’Keeffe, K.; Sar, G. K.; Anwar, M. S.; **Lizarraga, J. U. F.*; Aguiar, M. A. M. de***; Ghosh, D.

Swarmalators are oscillators that swarm through space as they synchronize in time. Introduced a few years ago to model many systems that mix synchrony with self-assembly, they remain poorly understood theoretically. Here, we obtain the first analytic results on swarmalators moving in two spatial dimensions by introducing a simplified model where the swarmalators have no hard-shell interaction terms and move on a periodic plane. These simplifications allow expressions for order parameters, stabilities and bifurcations to be derived exactly.

PROCEEDINGS OF THE ROYAL SOCIETY A-MATHEMATICAL PHYSICAL AND ENGINEERING SCIENCES 480[2301], 20240448, 2024. DOI: 10.1098/rspa.2024.0448

[P305-2024] “Advances on the Pierre Auger Outreach and Education program”

Cataldi, G. **Arbeletche, L. B.*; Chinellato, J. A.*; Franco, D de O.*; Dobrigkeit, C.*; Fauth, A. C.*; Payeras, A. M.***; **Reginatto Akim, J. V.***; et al.
Pierre Auger Observ Collaboration; Mokina V. (Ed.)

The Pierre Auger Observatory has implemented a novel method of astroparticle detection that combines various techniques and has an open data policy. The dissemination of information about the different astroparticle detection methods, ranging from surface water-Cherenkov detectors to underground scintillator detectors, is now possible due to access to specialized tools for data analysis. This allows for the introduction of the topic of astroparticles to teachers and students at different educational levels. This marks a significant moment for the Observatory. In this work, we will discuss the diverse outreach initiatives undertaken by the Observatory, which have facilitated interaction among members of the international collaboration and enabled collaborative actions between the permanent staff of the Observatory in Malargue and other institutions worldwide through synchronous meetings. These programs provide visitors with the opportunity to explore the environment of secondary particle cascades produced by cosmic rays, leading to a record number of monthly visitors since the opening of the Observatory 25 years ago.

XVIII INTERNATIONAL CONFERENCE ON TOPICS IN ASTROPARTICLE AND UNDERGROUND PHYSICS 324, 2024.

[P306-2024] “Analytical Calculations of Electron’s Phase Shift Due to Interactions with Magnetized Materials”

Soares, G. K.*; Muraca, D.*
IEEE

Differential phase contrast, through the use of transmission electron microscopes, allows accessing information on magnetic configurations or textures with resolutions smaller than nanometers and even close to angstroms depending on the characteristics of the microscope. This phenomenon is due to the Aharonov-Bohm effect, that predicts a shift in the relative phase (of the electron wave) between two beams traveling through different regions of the material, with electric or magnetic potentials. This shift can be used to make insights into the local magnetic configuration- contained in the region bounded by the beam paths. Here, we show how Toroidal Harmonics functions can be used to compute the phase shift generated by the magnetic vector potential for different geometries and magnetization textures with cylindrical symmetric geometries

IEEE INTERNATIONAL MAGNETIC CONFERENCE-SHORT PAPERS, INTERMAG SHORT PAPERS, 2024. DOI: 10.1109/icSmartGrid61824.2024.10576781

[P307-2024] “Anisotropy studies of ultra-high-energy cosmic rays measured at the Pierre Auger Observatory”

Schultec, J.; **Arbeletche, L. B.*; Chinellato, J. A.*; Franco, D de O.*; Dobrigkeit, C.*; Fauth, A. C.*; Payeras, A. M.***; **Reginatto Akim, J. V.***; et al.
Pierre Auger Collaboration. Mokina V. (Ed.)

Measurements of anisotropic arrival directions of ultra-high-energy cosmic rays provide important information for identifying their sources. On large scales, cosmic rays with energies above 8 EeV reveal a dipolar flux modulation in right ascension with a significance of 6.9 sigma, with the dipole direction pointing 113 degrees away from the Galactic center. This observation is explained by extragalactic origins. Also, model-independent searches for small- and intermediate-scale overdensities have been performed in order to unveil astrophysically interesting regions.

On these scales, no statistically significant features could be detected. However, intermediate-scale analyses comparing the measured arrival directions with potential source catalogs showindications for a coincidence of the measured arrival directions with catalogs of starburst galaxies and the Centaurus A region. In this contribution, an overview of the studies regarding anisotropies of the arrival directions of ultra-high-energy cosmic rays measured at the Pierre Auger Observatory on different angular scales is presented and the current results are discussed.

XVIII INTERNATIONAL CONFERENCE ON TOPICS IN ASTROPARTICLE AND UNDERGROUND PHYSICS 136, 2024.

[P308-2024] "Astrophysical interpretation of energy spectrum and mass composition of cosmic rays as measured at the Pierre Auger Observatory"

Guido, E.; **Arbeletche, L. B.*; Chinellato, J. A.*; Franco, D de O.*; Dobrigkeit, C.*; Fauth, A. C.*; Payeras, A. M.***; **Reginatto Akim, J. V.***; et al.
Pierre Auger Collaboration; Mokina V. (Ed.)

The combined interpretation of the spectrum and composition measurements plays a key role in the quest for the origin of ultra-high-energy cosmic rays (UHECRs). The Pierre Auger Observatory, thanks to its huge exposure, provides the most precise measurement of the energy spectrum of UHECRs and the most reliable information on their composition, exploiting the distributions of the depth of maximum of the showers in the atmosphere. A combined fit of a simple astrophysical model of UHECR sources to the spectrum and mass composition measurements is used to evaluate the constraining power of the data measured by the Pierre Auger Observatory on the source properties. We find that our data across the "ankle" feature are well reproduced if two extragalactic populations of sources are considered, one emitting a very soft spectrum which dominates the region below the ankle, and the other taking over at energies above the ankle, with an intermediate mixed composition, a hard spectrum and a low rigidity cutoff. Interestingly, similar results can also be obtained if the medium-mass contribution at lower energy is provided by an additional galactic component.

XVIII INTERNATIONAL CONFERENCE ON TOPICS IN ASTROPARTICLE AND UNDERGROUND PHYSICS, 125, 2024.

[P309-2024] "Experimentally Exploring the Performance of MOSFET Devices at Deep Cryogenic Temperatures"

Stucchi-Zucchi, L*.; Pavanello, M.; **Rouxinol, F.*; Diniz, J. A.***; Brito, F.
IEEE

This study investigates commercially available 180 nm CMOS devices under deep cryogenic conditions, focusing on both short (180 nm) and long (600 nm) channel nMOS devices at temperatures down to 3.2 K. We meticulously measured key parameters including threshold voltage (V-th), carrier mobility (mu n), subthreshold slope (SS), on-current (I-on), and off-current (I-off). Notably, as temperatures decreased, V-th, I-off, and SS values declined, while I-on and mu(n) exhibited an increase. A notable observation was the dual Z(t) values for the short channel device, aligning with the significant rise in series resistance post carrier freeze-out at 77 K. Our results provide a foundational understanding for the extraction of compact model parameters, crucial for cryogenic CMOS simulation and circuit design. For short channel devices, Vth evolved from 0.6 V at room temperature to 0.85 V at 3.8 K, carrier mobility increased from 200 to 400 cm(2)/V(2)s, and SS improved from 90 mV/dec to 20 mV/dec. Conversely, long channel devices, measured from 113 K to 3.2 K, showed V-th alteration from 0.60 V to 0.64 V, mobility enhancement from 833 to 1220 cm(2)/V(2)s, and SS improvement from 30 mV/dec to 10 mV/dec.

38TH SYMPOSIUM ON MICROELECTRONICS TECHNOLOGY AND DEVICES, SBMICRO, 2024. Série de livros: Microelectronics Technology and Devices. DOI: 10.1109/SBMicro64348.2024.10673862

[P310-2024] "First-Order Reversal Curve (FORC) Features of Ferrimagnetic and Antiferromagnetic Coupled Skyrmions"

Palhares, L.S.*; Batistel, T. M.*; Brandao, J.*; Béron, F.*
IEEE

This work aims to experimentally investigate probing coupled skyrmions in perpendicular magnetic anisotropy multilayers. The first-order reversal curve (FORC) method is a powerful technique to unveil hidden states or subtle behaviors in complex magnetic systems. We focus on two multilayer stacks aiming to antiferromagnetically coupled skyrmions to cancel the skyrmion Hall effect. In the first case, using a ferrimagnetic layer (CoGd/Pt), the skyrmions still present a non-null net magnetization. Helped by magnetic force microscopy, we found that with both high or low Dzyaloshinskii-Moriya interaction, skyrmions tend to merge with magnetic stripes. On the other hand, skyrmions in synthetic antiferromagnetic systems are fully compensated. By varying the spacer thickness in a Co/Pt/Ru multilayer, FORC results exhibit different features depending on the Co/Pt coupling, revealing a complex behavior.

IEEE INTERNATIONAL MAGNETIC CONFERENCE-SHORT PAPERS, INTERMAG SHORT PAPERS, 2024. DOI: 10.1109/INTERMAGSHORTPAPERS61879.2024.10576785

[P311-2024] "Interface Phenomena and Magnetic Hyperthemia of Fe 3 O Nanoparticles"

Alves, M. B.*; Almeida, A. A.*; Tancredi, P.*; Muraca, D.*
IEEE

Magnetic hyperthermia studies were carried out on different sizes magnetic nanoparticles of iron oxide (7.3 nm (7IOMNp) and 9.5 nm (9IOMNp)). Heat properties were correlated with morphological, structural (Transmission Electron Microscopy and X-ray Diffraction) and DC magnetic (SQUID-Super Quantum Interference Device) by means of magnetization loops and magnetization curves as function of temperature measured in the protocol zero-field-cooling and field-cooling (ZFC and FC curves). Based on obtained, the linear response model validity was analyzed to better understand the effects of magnetic hyperthermia varing frequency and intensity of applied magnetic field.

IEEE INTERNATIONAL MAGNETIC CONFERENCE-SHORT PAPERS, INTERMAG SHORT PAPERS, 2024. DOI: 10.1109/icSmartGrid61824.2024.10576772

[P312-2024] "Investigating Unusual Dynamics: Time and Frequency-Dependent Variations in Specific Power Absorption of Magnetite Nanoparticles in Magnetic Hyperthermia"

Silva, G. S. da*; Almeida, A. A. de*; Fabris, F.*; Muraca, D*.
IEEE

Magnetic hyperthermia is a mechanism that allows the conversion of electromagnetic field energy into heat by utilizing magnetic nanoparticles. To this, an external ac magnetic field, typically in the radiofrequency range, is applied to magnetic colloids containing magnetic monodomain nanoparticles resulting in the dissipation of heat energy into the surrounding medium. This work focuses on investigating iron oxide magnetic nanoparticles (IONPs), specifically Fe3O4 (magnetite), with diameters of 17 nm and 25 nm. Magnetic hyperthermia experiments,

conducted at frequencies between 150 kHz and 488 kHz with magnetic field amplitudes up to 550 Oe, revealed notable values of specific absorption rate (SAR), reaching 405 W/g for the 25 nm sample and 642 W/g for the 17 nm sample. Intriguingly, a reproducible increase in SAR was observed over time when applying the magnetic field, peaking at 768 W/g for the 17 nm sample, prompting ongoing investigation into its origin.

IEEE INTERNATIONAL MAGNETIC CONFERENCE-SHORT PAPERS, INTERMAG SHORT PAPERS, 2024. DOI: 10.1109/INTERMAGSHORTPAPERS61879.2024.10576815

[P313-2024] "Producing High-Ratio Nanowires by Pressure--Induced Infiltration into Anodized Aluminum Oxide Nanoporous Template"

Tomiatti, L.*; Mendonça, A. A.*; Béron, F.* et.al.
IEEE

This work aims to optimize the uniformity and filling factor of intermetallic nanowire arrays produced by the metallic flux nanonucleation into anodized aluminum oxide (AAO) templates. This technique allows the growth of a wide range of compositions, yielding a unique tool to achieve promising functional magnetic nanowires of high-quality. Since macroscopic magnetization characterization usually requires high magnetic signal and nanowire alignment, maximizing the template filling factor is crucial. We present a setup with objective of previously infiltrating the flux element into the nanopores, before performing the metallic flux protocol. It is based on an external applied pressure, under vacuum and heated conditions. We achieved throughout infiltration of Ga, a common flux element, in more than 71% of the nanopores (200 nm diameter and 80 mu m long) of an AAO template.

IEEE INTERNATIONAL MAGNETIC CONFERENCE-SHORT PAPERS, INTERMAG SHORT PAPERS, 2024. DOI: 10.1109/INTERMAGSHORTPAPERS61879.2024.10576909

[P314-2024] "Progress in nanofabrication of superconducting devices and diverse applications"

Rebello, A.; Klein, N. Y.; **Ruela, L. M.*;** Martins, E.; **Rouxinol, F.***; Oliveira, I. S.; Sinnecker, J. P.
IEEE

Superconducting circuits have emerged as a highly promising platform for quantum computing, among other divices based on Josephson junctions. The fabrication and testing of these devices requires especiallized nanofabrication facilities and milikelvin range testing equipment. In the search for the fabrication of these devices we have ran into limitations which forced us into creative solutions for the fabrications of these superconducting circuits and Josephson Junctions. Furthermore the development of these technologies allows for application in a wide range of research fields such as quantum computing, magnonics, micro-electromechanical systems and more.

IEEE INTERNATIONAL MAGNETIC CONFERENCE-SHORT PAPERS, INTERMAG SHORT PAPERS, 2024. DOI: 10.1109/INTERMAGSHORTPAPERS61879.2024.10576906

[P315-2024] Reducing Energy Waste by Tuning Martensite in Heusler Alloys"

Mendonça, A.*; Ghivelder, L.; Bernardo, P.; Cohen, L.; Gomes, A.
IEEE

Heusler alloys are widely studied due to their potential for practical applications, making use of their martensitic transformations. However, hysteresis is a long-standing drawback that reduces the chance of transferring these alloys from the laboratory to industry. In this work, we studied a Cr-doped Ni2MnGa-based material designed by integrating data obtained from the previous phase and hysteresis diagrams taken from the literature, reaching Ni2.15Mn0.70Cr0.15Ga. The compound presents a magnetostructural transition at room temperature, with a ferromagnetic martensite phase, and moderate thermal hysteresis of approximately 4 K. The magnetocaloric effect was explored, showing a reversible entropy change higher than 8 Jkg- 1K(-1) under 0-5 T field change, an advance towards high reversibility for this family alloys.

IEEE INTERNATIONAL MAGNETIC CONFERENCE-SHORT PAPERS, INTERMAG SHORT PAPERS, 2024. DOI: 10.1109/INTERMAGSHORTPAPERS61879.2024.10577074

[P316-2024] "Simulations of Experimentally Detected Ambient Skyrmions in Symmetric Synthetic Antiferromagnetic Multilayers"

Palhares, L.S.*; Batistel, T. M.*; Brandao, J.*; Béron, F*.
IEEE

Magnetic skyrmions are topological solitons consisting of non--collinear spin textures that display promising properties for spintronic information storage and logic devices. A type of system that has been proposed to host 2D skyrmions in room-temperature and zero magnetic field conditions, is the synthetic antiferromagnetic multilayer, composed of ferromagnetic layers that exhibit antiparallel RKKY coupling mediated by a non-magnetic spacer. In this work, we performed micromagnetic simulations to complement an experimental investigation about ambient skyrmions in Pt/Co/Ru/Co/Pt multilayers, assessing their magnetization reversal properties and coupled skyrmion stability.

IEEE INTERNATIONAL MAGNETIC CONFERENCE-SHORT PAPERS, INTERMAG SHORT PAPERS, 2024. DOI: 10.1109/INTERMAGSHORTPAPERS61879.2024.10576863

[P317-2024] "The CYGNO project for directional Dark Matter searches"

Amaro, F. D.; Antonietti, R.; Baracchini, E.; **Kemp, E.***; et al.
Mokina V. (Ed.)

The CYGNO project aims to develop a high-precision optical Time Projection Chamber (TPC) for directional Dark Matter search and solar neutrino spettroscopy, to be hosted at Laboratori-Nazionali del Gran Sasso (LNGS). The distinctive feature of CYGNO include the exploitation of scientific CMOS cameras and photomultiplier tubes coupled to a Gas Electron Multiplier for amplification within helium-fluorine-based gas mixture at atmospheric pressure. The primary objective of this project is to achieve three-dimentional tracking with head-tail capability and to enhance background rejection down to the keV energy range. This enhancement will significantly improve sensitivity to low Weakly Interacting Massive Particle masses for both Spin-Independent and Spin-Dependent coupling. We provide insights into the commissioning and underground operation of our 50-liter prototype, known as LIME, which represents the largest prototype developed by our collaboration to date. We showcase its capability to measure and identify low-energy nuclear and electron recoils. Additionally, we outline the design and prospects for the development of a funded O(1 m(3)) demonstrator, set to be housed in Hall F of LNGS. Furthermore, we present the physics potential that a future O(30 m(3)) experiment could bring to the field.

Lastly, we discuss the results from our collaboration's research and development efforts aimed at maximizing the potential of CYGNO. This includes the recent achievement of negative ion drift operation at atmospheric pressure with optical readout, which was accomplished in synergy with the ERC Consolidator Grant project INITIUM.

XVIII INTERNATIONAL CONFERENCE ON TOPICS IN ASTROPARTICLE AND UNDERGROUND 20, 2024.

[P318-2024] "Unlocking the Light(er) Sterile Neutrino Sector: Matter Effects and Mass Ordering"

Chattopadhyay, D. S.; Devi, M. M.; Dighe, A.; Dutta, D.; **Pramanik, D.*;** Raut, S.K.
Mokina V. (Ed.)

Future long-baseline experiments will be able to probe hitherto unexplored regions of sterile neutrino parameter space for masses ranging from meV to eV. We present an analytic calculation of the neutrino conversion probability P(ν mu -> ν(e)) in the presence of sterile neutrinos, with exact dependence on Delta m(41)(2) and matter effects. We further express the neutrino conversion probability as a sum of terms of the form sin (x) /x, thus allowing a physical understanding of matter effects and their possible resonance -like behavior. We focus on the identification of sterile mass ordering (sign of Amid at DUNE. The conversion probability obtained reveals the complex interplay between sterile and matter contributions. We perform numerical calculations of DUNE's sensitivity to sterile mass ordering over a broad range of sterile neutrino masses. Our analytic expressions enable us to explain the dependence of this sensitivity on Am241 values for all mass ordering combinations.

XVIII INTERNATIONAL CONFERENCE ON TOPICS IN ASTROPARTICLE AND UNDERGROUND PHYSICS. 283, 2024.

[P319-2024] "With AugerPrime to the Phase II of the Pierre Auger Observatory"

Martello, D.; **Arbeletche, L. B.*; Chinellato, J. A.*; Franco, D de O.*; Dobrigkeit, C.*; Fauth, A. C.*; Payeras, A. M.***; **Reginatto Akim, J. V.***; et al.
Pierre Auger Collaboration; Mokina V. (Ed.)

AugerPrime, the upgrade of the Pierre Auger Observatory, is nearing completion and the Observatory is now prepared to collect physics data after the commissioning of the new components. The Pierre Auger Observatory has demonstrated, based on the data collected thus far, the existence of the cutoff in the spectrum with high accuracy. However, the origin of this cutoff remains incompletely understood. The upgraded Observatory is designed to address the unresolved questions regarding the nature of the cosmic ray flux cutoff thanks to its capability to disentangle the muon and electromagnetic components of extensive air showers. Furthermore, the measurement of the muon component at ground level can verify the accuracy of hadronic interaction models currently used. This presentation will provide an overview of the status of the Observatory and the accurate commissioning done before the start of the physics run. Furthermore, we will present the initial data from Phase II data mainly dedicated to proving the continuity of operation of the Observatory from Phase I to Phase II.

XVIII INTERNATIONAL CONFERENCE ON TOPICS IN ASTROPARTICLE AND UNDERGROUND PHYSICS 123, 2024.

***Autores da comunidade IFGW**
Fonte: Web of Science on-line (WOS)

Defesas de Dissertações do IFGW

[D027-2024] "Propriedades de Transporte em Sistemas com Ordenamento Magnético e Interação Spin-Órbita"
Aluno: Alex Enrique Crispim
Orientador: Prof. Dr. Eduardo Miranda
Data: 02/12/2024

[D028-2024] "An EEG-based brain functional connectivity investigation of previously injured footballers"
Aluno: Pedro de Asevedo Piquet Carneiro
Orientador: Profa. Dra. Gabriela Castellano
Data: 18/12/2024

[D001-2025] "Sincronização de osciladores de Kuramoto em redes modulares"
Aluno: Leonardo Luís Bosnardo
Orientador: Prof. Dr. Marcus Aloizio Martinez de Aguiar
Data: 13/01/2025

Defesas de Teses do IFGW

[T017-2024] "Não-localidade de Bell multipartida e problemas de comunicação"
Aluno: Lucas da Silva Pollyceno
Orientador: Prof. Dr. Rafael Luiz da Silva Rabelo
Data: 17/12/2024

[T001-2025] "Desenvolvimento e Caracterização do MagLIte"
Aluno: Bruno Passarelli Gelli
Orientador: Prof. Dr. Ernesto Kemp
Data: 07/02/2025

Fonte: Portal IFGW/Eventos
Disponível em: https://portal.ifi.unicamp.br/a-instituicao/eventos/month.calendar/2023/12/14/-

Defesas de Dissertações e Teses do PECIM

***Sem atualização na página no período**

Fonte: Página do PECIM
Disponível em: https://www.pecim.unicamp.br/bancas

A Equipe BIF deseja
Boas Festas,
e que 2025 venha repleto de
boas energias, sabedoria
e esperanças renovadas!

Abstracta

Instituto de Física Gleb Wataghin - IFGW
Diretora: Profa. Dra. Mônica Alonso Cotta
Diretor Associado: Prof. Dr. Marcos Cesar de Oliveira
Universidade Estadual de Campinas - UNICAMP
Cidade Universitária Zeferino Vaz
13083-859 - Campinas - SP - Brasil
e-mail: secdir@ifi.unicamp.br
Fone: +55 19 3521-5300

Publicação

Biblioteca do Instituto de Física Gleb Wataghin
http://portal.ifi.unicamp.br/biblioteca
Instagram: @bif.unicamp

Diretora Técnica: Sandra Maria Carlos Cartaxo
Coordenadora da Comissão de Biblioteca: Profa. Dra. Arlene Cristina Aguilar

Elaboração e editoração:
Maria Graciele Trevisan (Bibliotecária)
Amélia Galdino Monteiro Amancio (Técnica)
Artes gráficas: Júlia da Silva Oliveira (Estagiária)
Contato: infobif@ifi.unicamp.br